# A Two-Stage Stochastic Optimization Planning Framework to Decarbonize Deeply Electric Power Systems

Luigi Boffino[a], Antonio J. Conejo[b,c], Ramteen Sioshansi[b,*], Giorgia Oggioni[d]

[a]*Sourcing & Portfolio Management, Engie Italia, S.p.A., via Chiese, 72, 20126 Milano, Italy*
[b]*Department of Integrated Systems Engineering, The Ohio State University, 1971 Neil Avenue, Columbus, Ohio 43210-1271, United States of America*
[c]*Department of Electrical and Computer Engineering, The Ohio State University, 2015 Neil Avenue, Columbus, Ohio 43210-1272, United States of America*
[d]*Department of Economics and Management, University of Brescia, Via S. Faustino 74/b-25122 Brescia, Italy*

**Abstract**

In 2015, 195 countries signed the Paris Agreement under the United Nations Framework Convention on Climate Change. To achieve the ambitious greenhouse gas-reduction targets therein, the electric power sector must be transformed fundamentally. To this end, we develop a two-stage stochastic optimization model. The proposed model determines the optimal mix of generation and transmission capacity to build to serve future demands at least cost, while respecting technical constraints and climate-related considerations. The model uses a mix of AC and high-voltage DC transmission lines, conventional and renewable generation, and different types of energy-storage units to meet these objectives. Short- and long-term uncertainties are modeled using operating conditions and scenarios, respectively.

We demonstrate the model using a case study that is based on the Texas power system, with 2050 as the target year of the analysis. We include explicit carbon-emissions constraints. Doing so allows us to examine the effect of carbon-reduction targets and deep decarbonization of electricity production on investment decisions. As expected, we find that thermal-dominated power systems must transition toward having a renewable-dominated generation mix.

*Keywords:* Generation-expansion planning, transmission-expansion planning, stochastic optimization, climate policy, energy storage
*JEL:* C61, C63, Q4, Q5

## 1. Introduction

As a result of concerns surrounding climate change, 195 countries signed the Paris Agreement under the United Nations Framework Convention on Climate Change in 2015. The agreement includes ambitious climate-related goals, which necessitate rapid and substantive declines in carbon emissions and the carbon-intensity of human activity. Moreover, a number of countries and regional international organizations have adopted carbon-reduction targets of their own. For instance, the European Union has adopted the so-called Energy Roadmap 2050, which includes targets to reduce greenhouse gas emissions by 80%–95% relative to 1990 levels by 2050.

Electricity production represents a major source of anthropogenic carbon emissions. Thus, the electric power system must play a substantive role in these reductions. Greater use of renewable energy sources, such as wind and solar, is one possible means of decarbonizing electricity production. However, the real-time availability of weather-dependent renewable energy sources is variable and uncertain. This gives rise

*Corresponding author
*Email addresses:* luigi.boffino@engie.it (Luigi Boffino), conejo.1@osu.edu (Antonio J. Conejo), sioshansi.1@osu.edu (Ramteen Sioshansi), giorgia.oggioni@unibs.it (Giorgia Oggioni)

to challenges in relying on such energy sources in place of dispatchable (*e.g.*, thermal) generation. Spatial disaggregation of renewables and energy storage are possible means to mitigate these issues that are caused by resource variability and uncertainty.

There are a number of works in the literature that examine decarbonization pathways for electric power systems and the role of renewables therein. Di Sbroiavacca et al. (2016) show how climate-related goals and carbon reductions could be achieved in the Argentinean electricity sector. Along the same lines, Calderón et al. (2016) examine decarbonization of the Colombian power system. They find that absent climate policy, $CO_2$ emissions increase for the foreseeable future with no stabilization. They show also that carbon-reduction goals can be achieved with greater use of renewable resources. Qi et al. (2016) examine how the carbon-intensity of electricity production in China declined between 2005 and 2013. The aim of their analysis is to inform future policy designs for further decarbonization of the Chinese power system.

Although these works demonstrate that renewables can play a significant role in decarbonizing electricity production, renewables create planning and operating challenges. As an example, Graf and Marcantonini (2017) conduct an empirical study of the operation of the Italian power system, using historical data from between 2005 and 2014. They show that renewables displaced thermal generation during this period, thereby reducing emissions. However, they find also that the variability in real-time renewable output increases cycling of thermal plants. This increased cycling reduces the operating efficiencies and increases slightly the emissions rates of the thermal plants. Nevertheless, there is a net emissions reduction from renewables during this period, as the former effect outweighs the latter.

Expanding upon the findings of Graf and Marcantonini (2017), achieving deep decarbonization of electricity production requires major changes in the generation mix. One must go beyond simply adding more renewables to a power system. Instead, the balance of the system must become more flexible to accommodate the variability of real-time renewable availability. Denholm et al. (2010) note that energy storage is expected to have a growing role as renewables constitute a larger portion of the generation mix. This is because energy storage can provide flexibility in shifting renewable generation through time, thereby managing its variability.

This paper adds to this existing literature by developing a modeling methodology to make generation- and transmission-planning decisions with decarbonization targets. Our model is formulated as a two-stage stochastic optimization problem wherein generation- and transmission-capacity planning decisions are made in the first stage. The second stage represents system operations during a set of representative operating days. These operating days capture implicitly short-term/small-scale uncertainties, such as load and renewable-supply variability. Long-term/large-scale uncertainties that are related to load growth are captured explicitly through scenarios that define the second stage of the stochastic optimization model.

Our model is formulated from the perspective of a central planner (*e.g.*, an integrated-resource planning process that is undertaken by an electric utility or a regulator). A number of jurisdictions have restructured electricity markets in place, meaning that this type of central-planning process does not occur. Nevertheless, our model is of value in such settings, as it can provide guidance on long-term planning decisions. Moreover, our modeling methodology provides insights as to how investments should be made by a risk-neutral agent that operates in a perfectly competitive restructured market. Despite our making these assumptions, agents are risk-averse in practice and markets for risk are incomplete and imperfect. de Maere d'Aertrycke et al. (2017) investigate the issue of incomplete risk trading and its impact on investments. They do this by analyzing stochastic equilibrium problems to quantify the impact of risk, market completeness, and contracting on generation investment while considering risk-mitigation instruments, such as contracts for differences, reliability options, and forward capacity markets. They show that these instruments are effective complements to an energy-only market, especially when they are managed by a regulator. While risk-related issues are important, they are beyond the scope of our work and are left for future study.

We focus our model development on representing two types of policies that can be implemented to decarbonize electricity production. One is an explicit cap on carbon emissions while the other is a carbon price. In this way our model can represent capacity expansion under current European climate policy and policies that have been contemplated in the United States. Our model accommodates a variety of technical approaches to decarbonization. This includes the use of renewable technologies, such as wind, photovoltaic (PV) solar, and concentrating solar power (CSP), nuclear generation, and fossil-fueled generation with carbon capture

and sequestration (CCS) systems. Our model allows AC and high-voltage DC (HVDC) transmission lines as well as well as stand-alone energy storage systems and integrating thermal energy storage (TES) into CSP plants. We demonstrate our model using a case study that is based on the Texas electric power system, using 2050 as the target planning year. Given the long planning horizon, we treat the system as having no generation capacity (insomuch as capacity that exists today is likely to be retired by 2050) but having existing transmission capacity (as such assets are long-lived). By changing the stringency of the decarbonization targets, we examine how the generation and transmission mixes change. We also examine a number of sensitivity cases, which show the impacts of changes in technology development and transmission congestion on the decarbonization pathway of the system. Although our results are specific to our Texas-based case study, we make a number of qualitative observations that are applicable broadly. Moreover, our modeling framework is sufficiently generic that it can be applied to determining decarbonization pathways for most power systems.

Our work makes two primary contributions to the existing literature. First, we propose a stochastic optimization framework that represents multi-scale uncertainties, AC and HVDC transmission, renewable generators, and energy-storage facilities. Also, we include in our model a novel representation of the operation of TES that is incorporated into CSP plants. Second, through our case study and sensitivity analyses, we examine the impacts of a variety of policy and technical factors on power system decarbonization. Specifically, we study the effects of environmental policies, investment mix, technology improvements, demand growth, and transmission-network congestion. We also examine trade-offs between the use of wind and solar generation for decarbonization.

The remainder of this paper is organized as follows. Section 2 details the proposed planning model. Section 3 summarizes our case-study data and provides more details on the technology options that are modeled in our analysis. Section 4 summarizes our case-study results in a base case, while Section 5 provides the results of our sensitivity analyses. Section 6 concludes.

## 2. Model

Our model follows the approach that is used by Liu et al. (2018b) in representing capacity-planning decisions. More specifically, we use a static two-stage stochastic investment model. The first stage concerns all of the generation- and transmission-investment decisions. The second stage captures all of the operating conditions. Long-term/large-scale uncertainties are represented explicitly in scenarios that define the second stage while short-term/small-scale uncertainties are captured implicitly via different representative operating conditions.

We proceed in this section by providing model notation first, which is followed then by a detailed model formulation. Then, we describe the technical and economic features that are captured in the model.

### *2.1. Model Notation*

#### *2.1.1. Indices*

| | |
|---|---|
| $c$ | Index of thermal generation units. |
| $g$ | Index of non-CSP renewable generation units. |
| $k$ | Index of CSP generation units. |
| $l$ | Index of existing and candidate transmission lines. |
| $n$ | Index of power system nodes. |
| $o$ | Index of operating conditions. |
| ref | Index for reference node. |
| $s$ | Index of stand-alone energy-storage units. |
| $t$ | Index of time periods within an operating condition. |
| $w$ | Index of scenarios. |
| $\tau$ | Index of final time period within an operating condition. |

Our model distinguishes two types of renewable and energy-storage technologies. The index, $k$, refers to CSP units, whereas the index, $g$, refers to non-CSP (*e.g.*, wind and PV solar) renewable generators. We

distinguish these two technology types because CSP units can include TES, which necessitates modeling these generators differently compared to other renewable technologies. In addition to the TES in CSP units, we also model stand-alone energy storage units, which are denoted by the index, $s$. This can include pure energy-storage technologies, such as electrochemical batteries, and hybrid energy-storage technologies, such as diabatic compressed-air energy storage (CAES). As discussed by Greenblatt et al. (2007); Succar et al. (2006); Succar and Williams (2008), diabatic CAES has different technical characteristics compared to pure energy storage, insomuch as it uses natural gas when being discharged (which entails $CO_2$ emissions and fuel costs). However, we represent the two types of technologies using the same generic approach.

*2.1.2. Sets*

| | |
|---|---|
| $\zeta^s(l)$ | Sending-end node of transmission line $l$. |
| $\zeta^r(l)$ | Receiving-end node of transmission line $l$. |
| $\Omega_n^C$ | Set of thermal units that are located at node $n$. |
| $\Omega_n^G$ | Set of non-CSP renewable units that are located at node $n$. |
| $\Omega_n^K$ | Set of CSP units that are located at node $n$. |
| $\Omega^{L+}$ | Set of candidate transmission lines. |
| $\Omega_a^{L+}$ | Set of candidate AC transmission lines. |
| $\Omega_n^S$ | Set of stand-alone energy-storage units that are located at node $n$. |

We divide the transmission lines into existing and candidate lines. This is because of our assumption that transmission-infrastructure investments are sufficiently long-lived that transmission corridors that are existing today are still operational in the future target year of the analysis (*i.e.*, 2050 in our case study). We subdivide the transmission lines into two technology types—AC and HVDC. The reason for this division is that power flows along the two types of lines are modeled differently. Power flows along AC transmission lines are represented using a linear approximation of Kirchhoff's laws. Power flows along HVDC lines are modeled using a 'pipeline assumption,' whereby power flows can be directed along each line. This is because each HVDC line is a radial connection between a single point in the AC transmission network and a candidate wind or CSP site.

We assume that there are no existing generation or energy-storage units in the target year of the analysis. This is because such assets are too short-lived for units that are operational today to be available in the target year. Thus, all thermal, wind, PV, CSP, and energy-storage units are in actuality candidate units that must be built to be available for operational use.

*2.1.3. Parameters*

| | |
|---|---|
| $b_{k,o,t}$ | Hour-$t$ capacity factor of CSP unit $k$ in operating condition $o$ [p.u.]. |
| $B_l$ | Susceptance of transmission line $l$ [S]. |
| $\bar{c}_k$ | Energy-storage capacity of TES system of CSP unit $k$ [h]. |
| $\bar{c}_s$ | Energy-storage capacity of stand-alone energy-storage unit $s$ [h]. |
| $f_{g,o,t}$ | Hour-$t$ capacity factor of non-CSP renewable unit $g$ in operating condition $o$ [p.u.]. |
| $F_l^{\max}$ | Capacity of transmission line $l$ [MW]. |
| $I_c^C$ | Investment cost of thermal unit $c$ [$/MW]. |
| $I^{C,\max}$ | Investment budget for building thermal units [$]. |
| $I_g^G$ | Investment cost of non-CSP renewable unit $g$ [$/MW]. |
| $I^{G,\max}$ | Investment budget for building non-CSP renewable units [$]. |
| $I_k^K$ | Investment cost of CSP unit $k$ [$/MW]. |
| $I^{K,\max}$ | Investment budget for building CSP units [$]. |
| $I_l^L$ | Investment cost of candidate transmission line $l$ [$]. |
| $I^{L,\max}$ | Investment budget for building candidate transmission lines [$]. |
| $I_s^S$ | Investment cost of stand-alone energy-storage unit $s$ [$/MW]. |
| $I^{S,\max}$ | Investment budget for building stand-alone energy-storage units [$]. |
| $M$ | A large fixed constant. |
| $P_{n,o,w,t}^{D,\max}$ | Hour-$t$ load at node $n$ in operating condition $o$ of scenario $w$ [MW]. |
| $\bar{P}_c^{C,\max}$ | Maximum capacity of thermal unit $c$ that can be built [MW]. |

$\bar{P}_g^{G,\max}$ Maximum capacity of non-CSP renewable unit $g$ that can be built [MW].
$\bar{P}_k^{K,\max}$ Maximum capacity of CSP unit $k$ that can be built [MW].
$\bar{P}_s^{S,\max}$ Maximum capacity of stand-alone energy-storage unit $s$ that can be built [MW].
$\beta_k$ Hourly energy-retention rate of TES system in CSP unit $k$ [p.u.].
$\beta_s$ Hourly energy-retention rate of stand-alone energy-storage unit $s$ [p.u.].
$\bar{\epsilon}$ Carbon-emissions limit [t].
$\epsilon_c$ Carbon-emissions rate of thermal unit $c$ [t/MWh].
$\epsilon_s$ Carbon-emissions rate of stand-alone energy-storage unit $s$ [t/MWh].
$\eta_k^K$ Charging efficiency of TES system in CSP unit $k$ [p.u.].
$\eta_s^S$ Roundtrip efficiency of stand-alone energy-storage unit $s$ [p.u.].
$\kappa_c^C$ Production cost of thermal unit $c$ [$/MWh].
$\kappa^D$ Load-shedding cost [$/MWh].
$\kappa_g^G$ Production cost of non-CSP renewable unit $g$ [$/MWh].
$\kappa_k^K$ Production cost of CSP unit $k$ [$/MWh].
$\kappa_k^{K,P}$ Charging cost of TES system of CSP unit $k$ [$/MWh].
$\kappa_k^{K,T}$ Discharging cost of TES system of CSP unit $k$ [$/MWh].
$\kappa_s^{S,P}$ Charging cost of stand-alone energy-storage unit $s$ [$/MWh].
$\kappa_s^{S,T}$ Discharging cost of stand-alone energy-storage unit $s$ [$/MWh].
$\xi_c^d$ Ramp-down limit of thermal unit $c$ [MW/h].
$\xi_c^u$ Ramp-up limit of thermal unit $c$ [MW/h].
$\rho_o$ Weight of operating condition $o$ [days].
$\phi_w$ Probability of scenario $w$.
$\chi$ Carbon-emissions price [$/t].

*2.1.4. Decision Variables*

$p_{c,o,w,t}^C$ Hour-$t$ production level of thermal unit $c$ in operating condition $o$ of scenario $w$ [MW].
$p_c^{C,\max}$ Capacity of thermal unit $c$ that is built [MW].
$p_{n,o,w,t}^D$ Hour-$t$ load at node $n$ that is shed in operating condition $o$ of scenario $w$ [MW].
$p_{g,o,w,t}^G$ Hour-$t$ production level of non-CSP renewable unit $g$ in operating condition $o$ of scenario $w$ [MW].
$p_g^{G,\max}$ Capacity of non-CSP renewable unit $g$ that is built [MW].
$p_{k,o,w,t}^K$ Hour-$t$ production level of CSP unit $k$ in operating condition $o$ of scenario $w$ [MW].
$p_k^{K,\max}$ Capacity of CSP unit $k$ that is built [MW].
$p_{l,o,w,t}^L$ Hour-$t$ power flow through transmission line $l$ in operating condition $o$ of scenario $w$ [MW].
$p_s^{S,\max}$ Capacity of stand-alone energy-storage unit $s$ that is built [MW].
$x_l^L$ Binary variable that equals 1 if candidate transmission line $l$ is built and equals 0 otherwise.
$\gamma_{k,o,w,t}^{K,L}$ Ending hour-$t$ state of charge (SOC) of TES system in CSP unit $k$ in operating condition $o$ of scenario $w$ [MWh].
$\gamma_{k,o,w,t}^{K,P}$ Hour-$t$ charging rate of TES system in CSP unit $k$ in operating condition $o$ of scenario $w$ [MW].
$\gamma_{k,o,w,t}^{K,T}$ Hour-$t$ discharging rate of TES system in CSP unit $k$ in operating condition $o$ of scenario $w$ [MW].
$\gamma_{s,o,w,t}^{S,L}$ Ending hour-$t$ SOC of stand-alone energy-storage unit $s$ in operating condition $o$ of scenario $w$ [MWh].
$\gamma_{s,o,w,t}^{S,P}$ Hour-$t$ charging rate of stand-alone energy-storage unit $s$ in operating condition $o$ of scenario $w$ [MW].
$\gamma_{s,o,w,t}^{S,T}$ Hour-$t$ discharging rate of stand-alone energy-storage unit $s$ in operating condition $o$ of scenario $w$ [MW].
$\theta_{n,o,w,t}$ Hour-$t$ phase angle at node $n$ in operating condition $o$ of scenario $w$ [rad].

*2.2. Model Formulation*

Our proposed two-stage stochastic planning model is formulated as:

$$\min \sum_c I_c^C p_c^{C,\max} + \sum_g I_g^G p_g^{G,\max} + \sum_k I_k^K p_k^{K,\max} + \sum_s I_s^S p_s^{S,\max} + \sum_{l\in\Omega^{L+}} I_l^L x_l^L \tag{1}$$
$$+ \sum_{w,o,t} \phi_w \rho_o \left\{ \sum_c \left(\kappa_c^C + \chi\epsilon_c\right) p_{c,o,w,t}^C + \sum_n \kappa^D p_{n,o,w,t}^D + \sum_g \kappa_g^G p_{g,o,w,t}^G \right.$$
$$\left. + \sum_k \left(\kappa_k^K p_{k,o,w,t}^K + \kappa_k^{K,P}\gamma_{k,o,w,t}^{K,P} + \kappa_k^{K,T}\gamma_{k,o,w,t}^{K,T}\right) + \sum_s \left[\kappa_s^{S,P}\gamma_{s,o,w,t}^{S,P} + \left(\kappa_s^{S,T} + \chi\epsilon_s\right)\gamma_{s,o,w,t}^{S,T}/\eta_s^S\right] \right\}$$

$$\text{s.t. } 0 \le p_c^{C,\max} \le \bar{P}_c^{C,\max}, \quad \forall c \tag{2}$$
$$0 \le p_g^{G,\max} \le \bar{P}_g^{G,\max}, \quad \forall g \tag{3}$$
$$0 \le p_k^{K,\max} \le \bar{P}_k^{K,\max}, \quad \forall k \tag{4}$$
$$0 \le p_s^{S,\max} \le \bar{P}_s^{S,\max}, \quad \forall s \tag{5}$$
$$x_l^L \in \{0,1\}, \quad \forall l \in \Omega^{L+} \tag{6}$$
$$\sum_c I_c^C p_c^{C,\max} \le I^{C,\max} \tag{7}$$
$$\sum_g I_g^G p_g^{G,\max} \le I^{G,\max} \tag{8}$$
$$\sum_k I_k^K p_k^{K,\max} \le I^{K,\max} \tag{9}$$
$$\sum_s I_s^S p_s^{S,\max} \le I^{S,\max} \tag{10}$$
$$\sum_{l\in\Omega^{L+}} I_l^L x_l^L \le I^{L,\max} \tag{11}$$
$$\sum_{w,o,t} \phi_w \rho_o \left(\sum_c \epsilon_c p_{c,o,w,t}^C + \sum_s \epsilon_s \gamma_{s,o,w,t}^{S,T}\right) \le \bar{\epsilon} \tag{12}$$
$$\sum_{c\in\Omega_n^C} p_{c,o,w,t}^C + \sum_{g\in\Omega_n^G} p_{g,o,w,t}^G + \sum_{k\in\Omega_n^K} \left(p_{k,o,w,t}^K - \gamma_{k,o,w,t}^{K,P} + \gamma_{k,o,w,t}^{K,T}\right) - \sum_{s\in\Omega_n^S} \left(\gamma_{s,o,w,t}^{S,P} - \gamma_{s,o,w,t}^{S,T}/\eta_s^S\right) \tag{13}$$
$$+ \sum_{l,\zeta^r(l)=n} p_{l,o,w,t}^L - \sum_{l,\zeta^s(l)=n} p_{l,o,w,t}^L = P_{n,o,w,t}^{D,\max} - p_{n,o,w,t}^D, \quad \forall n,o,w,t$$
$$0 \le p_{c,o,w,t}^C \le p_c^{C,\max}, \quad \forall c,o,w,t \tag{14}$$
$$-\xi_c^d \le p_{c,o,w,t}^C - p_{c,o,w,t-1}^C \le \xi_c^u, \quad \forall c,o,w,t>1 \tag{15}$$
$$0 \le p_{g,o,w,t}^G \le f_{g,o,t} p_g^{G,\max}, \quad \forall g,o,w,t \tag{16}$$
$$0 \le p_{k,o,w,t}^K + \gamma_{k,o,w,t}^{K,P} \le b_{k,o,t} p_k^{K,\max}, \quad \forall k,o,w,t \tag{17}$$
$$0 \le \gamma_{k,o,w,t}^{K,P} \le b_{k,o,t} p_k^{K,\max}, \quad \forall k,o,w,t \tag{18}$$
$$0 \le p_{k,o,w,t}^K + \gamma_{k,o,w,t}^{K,T} \le p_k^{K,\max}, \quad \forall k,o,w,t \tag{19}$$
$$0 \le \gamma_{k,o,w,t}^{K,T} \le p_k^{K,\max}, \quad \forall k,o,w,t \tag{20}$$
$$\gamma_{k,o,w,t}^{K,L} = \beta_k \gamma_{k,o,w,t-1}^{K,L} + \eta_k^K \gamma_{k,o,w,t}^{K,P} - \gamma_{k,o,w,t}^{K,T}, \quad \forall k,o,w,t \tag{21}$$
$$0 \le \gamma_{k,o,w,t}^{K,L} \le \bar{c}_k p_k^{K,\max}, \quad \forall k,o,w,t \tag{22}$$
$$0 \le \gamma_{s,o,w,t}^{S,P} \le p_s^{S,\max}, \quad \forall s,o,w,t \tag{23}$$

$$0 \leq \gamma^{S,T}_{s,o,w,t}/\eta^{S}_{s} \leq p^{S,\max}_{s}, \quad \forall s,o,w,t \tag{24}$$

$$\gamma^{S,L}_{s,o,w,t} = \beta_s \gamma^{S,L}_{s,o,w,t-1} + \gamma^{S,P}_{s,o,w,t} - \gamma^{S,T}_{s,o,w,t}, \quad \forall s,o,w,t \tag{25}$$

$$0 \leq \gamma^{S,L}_{s,o,w,t} \leq \bar{c}_s p^{S,\max}_{s}, \quad \forall s,o,w,t \tag{26}$$

$$\gamma^{S,L}_{s,o,w,\tau} \geq \gamma^{S,L}_{s,o,w,0} = 0.5 p^{S,\max}_{s}, \quad \forall s,o,w \tag{27}$$

$$-F^{\max}_{l} \leq p^{L}_{l,o,w,t} \leq F^{\max}_{l}, \quad \forall l \notin \Omega^{L+}, o,w,t \tag{28}$$

$$-F^{\max}_{l} x^{L}_{l} \leq p^{L}_{l,o,w,t} \leq F^{\max}_{l} x^{L}_{l}, \quad \forall l \in \Omega^{L+}, o,w,t \tag{29}$$

$$p^{L}_{l,o,w,t} = B_l \cdot \left(\theta_{\zeta^s(l),o,w,t} - \theta_{\zeta^r(l),o,w,t}\right), \quad \forall l \notin \Omega^{L+}, o,w,t \tag{30}$$

$$-\left(1 - x^{L}_{l}\right) M \leq p^{L}_{l,o,w,t} - B_l \cdot \left(\theta_{\zeta^s(l),o,w,t} - \theta_{\zeta^r(l),o,w,t}\right) \leq \left(1 - x^{L}_{l}\right) M, \quad \forall l \in \Omega^{L+}_{a}, o,w,t \tag{31}$$

$$-\pi \leq \theta_{n,o,w,t} \leq \pi, \quad \forall n,o,w,t \tag{32}$$

$$\theta_{\text{ref},o,w,t} = 0, \quad \forall o,w,t \tag{33}$$

$$0 \leq p^{D}_{n,o,w,t} \leq P^{D,\max}_{n,o,w,t}, \quad \forall n,o,w,t. \tag{34}$$

Objective function (1) consists of total investment and expected operation cost of the power system. We assume that the investment-cost parameters, $I^C_c$, $I^G_g$, $I^K_k$, $I^S_s$, $I^L_l$, are annualized to make the investment and operations costs comparable to one another. Otherwise, the costs would be skewed because the investments are long-lived while operations may only be modeled over a short duration (*e.g.*, for a single representative year in our case study). The simplest way to annualize the investment costs is to multiply the overnight cost of building each technology by:

$$\frac{i \cdot (1+i)^y}{(1+i)^y - 1},$$

where $y$ is the assumed lifetime of the asset and $i$ is the real interest rate.

Operating costs are computed in each hour of each operating condition of each scenario. These operating costs include the costs of producing energy from the thermal and renewable generators, the costs of operating the TES that is embedded in the CSP units and the stand-alone energy-storage units, and the costs of any load curtailments.

We also include operating costs that are associated with $CO_2$ emissions (*e.g.*, due to a Pigouvian-tax or cap-and-trade policy). We assume two possible sources of $CO_2$ emissions—thermal generators and stand-alone energy-storage units. Any fossil-fueled thermal generator that does not have a CCS system incorporated in it will release $CO_2$. Diabatic CAES also releases $CO_2$ when it is discharged, which is associated with the combustion of natural gas. Thus, we allow for cases in which the use of energy-storage units can result in $CO_2$ emissions. We also examine, in two of our sensitivity cases in Sections 5.4 and 5.5, the viability of battery energy storage (BES) and adiabatic CAES, which are pure energy-storage technologies, the uses of which do not entail any direct $CO_2$ emissions.

The model has two types of constraints. Constraints (2)–(12) pertain to the first (investment) stage while the remaining pertain to the second (operating) stage. Constraints (2)–(5) impose capacity limits on how much thermal, CSP and non-CSP renewable, and energy-storage capacity can be built at each candidate location. These constraints may reflect land-use, resource, or other physical limitations on the deployment of these units. Constraints (6) impose the binary nature of transmission-expansion decisions, which have this 'lumpy' nature. Constraints (7)–(11) impose budget constraints on the investment decisions. Constraint (12) imposes an expected carbon-emissions limit (*e.g.*, due to a cap-and-trade system limiting total system emissions). As such, our model captures two common means of imposing carbon-emissions limits. One is an explicit limit, as imposed by Constraint (12), while the other is a more implicit cost or tax on carbon emissions, which is captured in Objective function (1). In practice, policy makers may focus on implementing one of these types of policy mechanisms as opposed to both.

Constraints (13) impose nodal load balance in each operating period. Constraints (14) and (15) impose capacity and ramping limits, respectively, on the operation of the thermal units. Constraints (16) impose capacity constraints on the output of the non-CSP renewable units. The energy that is available to be produced in each operating period is represented using a capacity factor, which captures the impact of

weather conditions. The same approach is used to represent the impact of weather on energy that is available from CSP plants.

Constraints (17)–(22) pertain to the operation of the CSP units. We model the CSP units by adapting the methodology that is developed by Sioshansi and Denholm (2010a,b). Constraints (17) restrict the total amount of energy that each CSP unit produces and stores in its TES system to be no greater than the amount of energy that is collected by the unit's solar field. The energy that is collected by a CSP plant's solar field is thermal. As such, we apply the assumed powerblock efficiency to convert the thermal energy into the equivalent amount of electrical energy that would be produced by the CSP unit when the stored energy is discharged. Doing so allows for more streamlined modeling of the CSP unit and its integrated TES system within a planning model. Constraints (18) ensure that the TES system does not store more than its power capacity allows. Constraints (19) limit the total production of each CSP unit, either by using directly energy from its solar field or from its TES system, to be no greater than the power capacity of its powerblock. Constraints (20) limit the amount of energy that is discharged from the TES system based on its power capacity. Constraints (21) define how the SOC of the TES system in each CSP unit evolves from one operating period to the next. Finally, Constraints (22) impose energy limits on the SOC of the TES system in each CSP unit.

Constraints (23)–(27), which are adapted from the works of Drury et al. (2011); Sioshansi et al. (2009), describe the operation of the stand-alone energy-storage units. Constraints (23)–(24) impose power-capacity limits on the charging and discharging, respectively, of energy-storage units. Constraints (25) define how the SOC of each energy-storage unit changes from one operating period to the next and Constraints (26) impose energy limits on the SOC. Constraints (27) fix the SOC of each energy-storage unit at the beginning of each operating condition (which are taken to be representative operating days in our case study) to 50% of its energy capacity. These constraints also require the SOC of energy-storage unit to be above this level at the end of each operating condition. Graves et al. (1999) suggest this as a heuristic technique to ensure that a model does not deplete fully energy storage at the end of each optimization horizon.

Constraints (28) impose power-flow limits on each existing transmission line while Constraints (29) do the same for candidate lines. These latter constraints also force the power flow on a candidate transmission line that is not built to equal zero, which is a physical requirement. Constraints (30) define power flows on existing transmission lines in terms of differences in the phase angles at the two ends of the line. Constraints (31) define power flows on candidate transmission lines analogously. These latter constraints are written in this inequality form to allow the flows on a candidate transmission line that is not built to equal zero without forcing the phase angles at the two ends of that line to equal one another. This is a standard approach to modeling power flows with binary transmission-investment decisions. Conejo et al. (2016) provide further details on how these constraints are modeled. Power flows in HVDC lines are not modeled using phase angles. Rather, because these lines are radial connections to distant candidate wind or CSP sites, their power flows can be set arbitrarily within their bounds without impacting power flows elsewhere in the network. Constraints (32) impose limits on the phase angles and Constraints (33) fix the phase angles at the reference node to be zero.

Finally, Constraints (34) limit the amount of load that is curtailed at each node to be no greater than the nodal demand.

Our proposed capacity-expansion model is a mixed-integer linear optimization problem. Thus, it can be solved tractably using off-the-shelf commercial software tools, such as CPLEX or Gurobi. Although we have a stochastic optimization problem, explicit non-anticipativity constraints are not needed. This is because the investment decisions (*i.e.*, $p_c^{C,\max}$, $p_g^{G,\max}$, $p_k^{K,\max}$, $p_s^{S,\max}$, and $x_l^L$) are defined so as not to depend on the realization of the second-stage scenarios, $w$. The proposed model can also be used in a rolling-horizon fashion over time, whereby future scenarios are updated periodically (*e.g.*, the model can be re-run every year with updated scenarios of future conditions). Domínguez et al. (2015) argue that using a two-stage stochastic planning model in such a manner can yield solutions that are similar to those that are achieved using a more computationally costly multi-period model.

## 3. Case-Study Data

Our case study considers a 28-node system, which is a modified version of the IEEE 24-node test system. The topology of the network and other system data are adapted from the Electric Reliability Council of Texas (ERCOT) power system. However, loads and generator and transmission-lines capacities are scaled down so as to keep the reference load at 3.7 GW in the base case. We focus our case study on ERCOT because it is mostly an electrically isolated power system (with the exception of some limited DC tie lines to neighboring interconnects) with substantial load and potential for the deployment of renewables.

Figure 1 shows the topology of the network. Generating and energy-storage units that are available to be built in the base case are labeled in the figure based on how they are indexed in the model formulation (*i.e.*, $c$, $k$, $g$, and $s$ for thermal, CSP and non-CSP renewable, and stand-alone energy-storage units, respectively). Existing transmission lines are indicated by solid lines whereas candidate AC lines are indicated by dashed lines. Dotted lines indicate candidate HVDC lines. Loads are indicated by arrows.

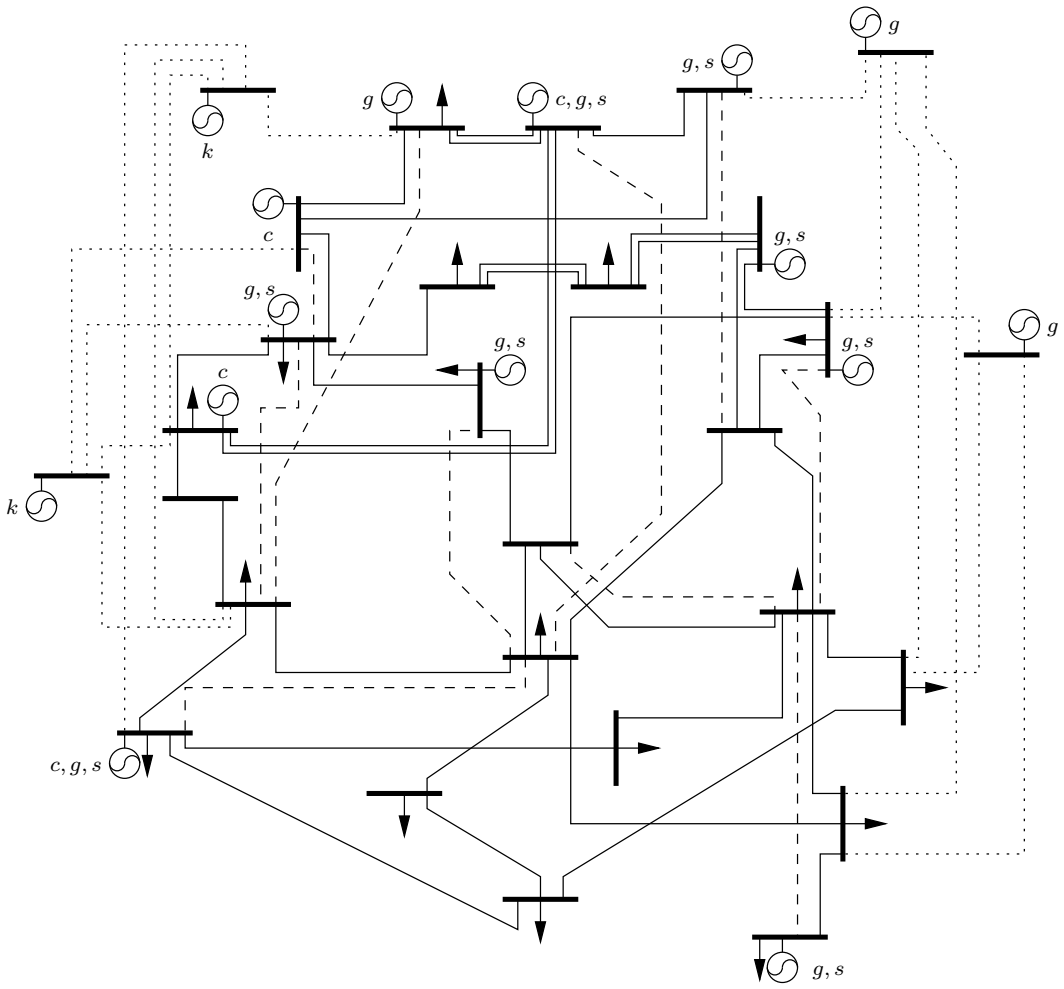


Figure 1: 28-Node Network Diagram

Twenty-four of the nodes represent the center of the network where the loads and most of the candidate generating and energy-storage units are located. As such, these nodes are connected by existing AC lines and candidate AC lines can be built to reinforce connections within the center of the network. The remaining nodes are isolated and can be connected to the center of the network with candidate HVDC lines. Two of

the nodes are candidate locations for offshore-wind generators while the other two are candidate locations for CSP plants.

Our case study includes 63 candidate units: 40 thermal, 11 onshore wind, two offshore wind, two CSP, and eight stand-alone energy-storage units. Additional candidate CSP units are considered in one of the sensitivity cases that is examined in Section 5.3. A sensitivity case in Section 5.4 also adds ten candidate PV generators that are co-located with ten candidate BES units. Our base case explores specifically the extent to which major load centers across a region can be supplied by highly efficient renewable resources that are located sufficiently far away from the load pockets that costly HVDC links are required. These highly efficient renewable resources include both offshore-wind units[1] and CSP.[2] CAES energy storage units can also be used to maximize the utilization of these weather-dependent renewable resources and manage their variability.

We consider ten different thermal generation technologies: advanced pulverized coal units (with and without CCS), conventional natural gas-fired combined cycle (NGCC) units, advanced NGCC units (with and without CCS), conventional and advanced natural gas-fired combustion turbines (CT), integrated gasification combined cycle (IGCC) units (with and without CCS), and advanced nuclear units. This represents generating technologies that, as reported by the United States Energy Information Administration (EIA),[3] are available today or that are anticipated to be available commercially by the target year of our analysis (2050).

Table 1 summarizes the cost, maximum-capacity, and emissions-rate data for the thermal units, which are obtained from the EIA. All of the technologies are assumed to be able to ramp over their full output range, with the exception of nuclear units, which are assumed to have no ramping capability. Instead, nuclear units are assumed to operate continuously at their installed capacities as must-run units. The operating costs that are reported in Table 1 are computed using projections of future fuel prices that are published by EIA (2017). The maximum capacity for each technology that is reported in Table 1 is the total amount that can be installed across all of the candidate locations where that technology can be built.

Table 1: Data For Candidate Thermal Units

| Technology | Investment Cost [$/kW] | Operating Cost [$/MWh] | Maximum Capacity [MW] | $\epsilon_c$ |
|---|---|---|---|---|
| Advanced Pulverized Coal without CCS | 2933 | 25.95 | 3800 | 0.841 |
| Advanced Pulverized Coal with CCS | 5227 | 38.15 | 3800 | 0.112 |
| Conventional NGCC | 917 | 46.82 | 2880 | 0.374 |
| Advanced NGCC without CCS | 1023 | 42.69 | 2400 | 0.341 |
| Advanced NGCC with CCS | 2095 | 52.91 | 2160 | 0.041 |
| Conventional CT | 973 | 81.97 | 1600 | 0.576 |
| Advanced CT | 676 | 70.14 | 2400 | 0.518 |
| IGCC without CCS | 3784 | 26.19 | 3800 | 0.743 |
| IGCC with CCS | 6599 | 33.22 | 3000 | 0.097 |
| Advanced Nuclear | 5530 | 16.06 | 4800 | 0.000 |

There are 11 candidate locations, which are in the center of the test system, for onshore wind. Conversely, offshore wind can only be built at two nodes that are isolated from the center of the system. Onshore wind has investment costs that range between $1970/kW and $2100/kW and operating costs that range between $2.00/MWh and $2.71/MWh. A maximum of 7700 MW of wind can be built at the onshore sites. Up to 4000 MW of offshore wind can be built. These units have higher investment costs that range between $2900/kW and $3190/kW, which reflects the greater complexity that installing offshore wind entails. These

[1] https://www.tennet.eu/our-key-tasks/innovations/north-sea-wind-power-hub/
[2] https://theconversation.com/should-we-turn-the-sahara-desert-into-a-huge-solar-farm-114450
[3] https://www.eia.gov/analysis/studies/powerplants/capitalcost/

units also have higher operating costs that range between \$4.85/MWh and \$5.35/MWh, which reflects the greater challenges in their operation and maintenance. One of the candidate offshore-wind units is closer to the shore, which results in its having a lower investment cost (and a lower cost for building the associated HVDC line that connects it to the center of the network). The other offshore-wind unit is further from the coast, giving it a higher average capacity factor and lower operating cost. Investment and operating costs of the wind units are obtained from the EIA and the work of Krohn et al. (2009).

Up to 2000 MW total of CSP capacity can be built across the two candidate locations. We assume that the solar field of each CSP plant is scaled to maintain a solar multiple of 2.0. A CSP plant with a solar multiple of 2.0 is sized to provide sufficient thermal energy to operate the powerblock at its rated capacity with a direct normal irradiance of 950 W/m$^2$, a 5-m/s wind speed, and a 25-C ambient temperature. Furthermore, we assume that each CSP plant has a TES system with $\bar{c}_k = 4$ hours of storage capacity. This means that a fully charged TES system can be discharged and operated at its nameplate capacity for four consecutive hours.[4] Operating and investment costs for the CSP units are obtained from version 2017.1.17 of System Advisor Model (SAM). Blair et al. (2014) provide a general overview and description of SAM. We assume power-tower CSP systems with investment costs ranging between \$3272/kW and \$3599/kW and generation costs ranging between \$3.80/MWh and \$4.00/MWh. The TES systems in the CSP plants are assumed to have operating costs of \$0.1400/MWh in charging mode and \$0.1549/MWh in discharging mode. We assume that the TES systems have a 99% roundtrip efficiency and 0.1% hourly thermal-energy losses, meaning that we have $\eta_k^K = 0.99$ and $\beta_k = 0.999$ for all $k$. As with the offshore-wind units, one of the candidate CSP units is assumed to be closer to a load pocket in the system, meaning that this unit has a lower cost of being connected to the system with HVDC lines. However, this unit has a lower average capacity factor than the other CSP unit.

Our base case considers a single stand-alone energy-storage technology, which is diabatic CAES. Diabatic CAES is a hybrid energy-storage technology that uses both electricity (to compress air) and natural gas (when stored energy is discharged). When charged, electricity is used to drive a compressor, which injects pressurized air into a reservoir. When discharged, the compressed air is withdrawn from the reservoir and combined with natural gas in an open-cycle combustion turbine. Combustion produces high-pressure gas, which is expanded through a turbine, that drives both an electric generator and the air compressor. The benefit of using the compressed air in the discharging phase is that the combustion turbine has a heat rate of approximately 4200 BTU/kWh,[5] which is half that of a conventional CT. Because diabatic CAES is a hybrid energy-storage technology, only 0.7 MWh of stored electric energy must be used to discharge 1 MWh of electricity. Adiabatic CAES, further details of which are given in Section 5.5, and BES are considered in two of the sensitivity cases. Like BES, adiabatic CAES is a pure energy-storage technology, which does not entail the combustion of any fossil fuel when discharged.

Sioshansi et al. (2011) note that CAES is an attractive large-scale energy-storage technology with long life expectancy, low investment and maintenance costs, and reasonable roundtrip efficiency. Moreover, Succar and Williams (2008) find that many areas of the world that are well suited for the deployment of CAES are also wind-rich. This includes ERCOT. This can be contrasted with the (currently) more commonly used pumped hydroelectric storage (PHS) technology, which requires access to water and reservoirs at different elevations. Water is scarce and the requisite geological formations are lacking in many wind-rich areas of the world, including in Texas.

We model eight candidate CAES units. Each CAES unit is assumed to have a fixed $\bar{c}_s = 10$ hours of storage capacity. Each CAES units can be built with up to 350 MW of power capacity. We take operating and investment costs and physical properties of the CAES plants from the work of Das et al. (2011). We assume that the investment costs range between \$550/kW and \$610/kW and that each CAES unit has an operating cost of \$0.50/MWh when charging energy. The discharging costs range between \$28.33/MWh and

[4] In actuality, a fully charged TES system would operate very slightly below 100% of its nameplate capacity in the fourth hour. The reason for this is that the TES system incurs small thermal-energy losses from one hour to the next. Thus, the four-hour definition is based on an assumption of no thermal-energy losses.

[5] We report this heat rate in imperial (as opposed to SI) units, as BTU/kWh is still the most commonly used unit of generator efficiency in the United States.

$28.79/MWh, which reflect primarily the cost of natural gas. Each CAES unit is also assumed to have a carbon-emissions rate of 0.259 t/MWh and an efficiency of $\eta_s^S = 0.7$ (based on the characteristic that only 0.7 MWh of stored energy must be used to discharge 1 MWh of electricity).

The transmission system consists of 38 existing lines, which range in capacity from 200 MW to 800 MW and have an average capacity of about 440 MW. These existing lines are all AC and connect the nodes in the center of the network. Ten candidate AC lines, with capacities ranging between 400 MW and 800 MW, can be added to create further links amongst the nodes in the center of the network. There are a further 15 candidate HVDC lines, which only connect one of the four remote nodes to one of the nodes in the center of the network. Each of the distant nodes has multiple candidate HVDC lines with which it can be connected to the main grid, indicating that a particular offshore-wind or CSP project has multiple potential points of interconnection with the main network. Eight of the HVDC lines have a 2-GW capacity while the remainder have a 1-GW capacity. Transmission-investment costs are obtained from the work of Vaillancourt (2014).

We annualize the investment costs by assuming a 25-year depreciation period and a 10% real interest rate. This yields an 11% cost-annualization rate.

We model different load and wind- and solar-availability conditions using scenarios and operating conditions. Specifically, we represent operations in the target year through a set of operating conditions, which are indexed by $o$ in the model. Each operating condition is taken to be a representative day, which is modeled at hourly time steps (*i.e.*, the index, $t$, corresponds to the 24 hours of each representative day). We use the scenarios, which are indexed by $w$ in the model, to capture uncertainty in long-term demand growth between today and 2050.

To capture correlations in wind and solar availabilities and load, the operating-condition data are all obtained using historical data from the year 2012. Historical load data are obtained from ERCOT and scaled to obtain reference loads for the system. These reference loads are apportioned to the nodes (*cf.* Figure 1) based on the historical distribution of loads to different zones of the ERCOT network.

Wind-speed data are obtained from the Wind Integration National Dataset (WIND) Toolkit. Draxl et al. (2015a,b) provide details and meteorological validation of the WIND Toolkit. Wind speeds are used to determine the real-time availability of wind power, which is represented in the model through the capacity factors, $f_{g,o,t}$. King et al. (2014) validate the use of the WIND Toolkit for this type of simulation. We collect wind-speed data for 33 onshore locations and for the representative southwestern Texas offshore location. The wind-speed data are then processed using SAM, assuming the power curve of a 2-MW Vestas V80/2000 wind turbine with an 80-m hub height to generate hourly wind-availability data. Wind-availability profiles for the 13 candidate wind locations are obtained by spatial averaging of the profiles from the locations in the WIND Toolkit that are used.

Solar availabilities are simulated using SAM, based on weather data that are obtained from the National Solar Radiation Database (NSRDB). Sengupta et al. (2014a,b) provide details and validation of the NSRDB data. We consider only two candidate CSP plants in our base case. As such, we use NSRDB data for five locations that are in relatively close proximity to one another to simulate the solar-availability of each CSP plant (*i.e.*, we use NSRDB data for 10 locations total). We use SAM to simulate the operation of a standard power-tower CSP plant with a 110-MW powerblock, a solar multiple of 2.0, and a TES system with 100 hours of storage capacity. From this simulation, we can determine the maximum amount of thermal energy that is captured by the CSP plant in each hour (*i.e.*, the 100-hour TES system ensures that no thermal energy is curtailed in the SAM simulation due to power constraints on the operation of the plant). We then use the assumed 41.2% average efficiency of the CSP plant's powerblock to convert the simulated thermal energy that is captured by the solar field in each hour to the amount of equivalent electrical energy that would be produced by the powerblock. Finally, we normalize the potential electrical output by the 110-MW nameplate capacity of the powerblock to obtain hourly capacity factors for each CSP plant that is simulated in SAM. Again, we use spatial averaging to convert these capacity factors to the capacity factors for each of the two candidate CSP plants that are used in our planning model. Depending on ambient weather conditions, the capacity factor of a CSP plant can be greater than unity in some hours, indicating that the solar field collects more thermal energy than can be utilized by the powerblock. Such excess energy can be stored in the TES system.

Once we have a full set of load and wind- and solar-availability data for the year, we use $k$-means clustering to reduce the full year into a set of representative operating days. Thus, we obtain our final set of operating conditions (*i.e.*, the set over which the index, $o$, in our model is defined) from this process. MacQueen (1967) is a formative work that describes the $k$-means clustering algorithm, while Baringo and Conejo (2013); Liu et al. (2018a) describe its use in obtaining operating conditions that represent annual load, wind, and solar patterns and respect their auto- and cross-correlations. The $k$-means clustering algorithm provides 15 clusters, each of which gives one representative day for the planning model (*i.e.*, our planning model has 15 day-long operating conditions). The load, wind, and solar data for the operating condition that is used to represent each cluster are obtained from the day within the cluster that is closest to the cluster centroid. We assign a weight to the representative day (*i.e.*, the value of $\rho_o$ in the planning model) that is equal to the number of days within its associated cluster. This clustering results in the system having a peak load of 3.1 GW in the base scenario of the scenario tree.

In addition to short-term uncertainty in load and renewable availability, we model demand growth as a source of long-term uncertainty. Demand growth is represented explicitly via second-stage scenarios in the scenario tree. We assume that with probability 0.5 the demands are equal to the values that are obtained from the $k$-means clustering (*i.e.*, this is a 'no-demand-growth' scenario). With probability 0.3 demands are assumed to grow an additional 5% relative to this baseline value (*i.e.*, a high-demand scenario) and with probability 0.2 demands are 3% lower (*i.e.*, a low-demand scenario). One reason for modeling uncertain demand growth is that it 'forces' the model to build sufficient capacity to serve higher-than-expected demands. This excess capacity that the demand-growth scenarios engender can be analogized to planning-reserve margins, which are enforced normally as constraints in deterministic capacity-expansion models. A benefit of modeling demand-growth scenarios (as opposed to planning-reserve margins) is that the objective function takes into account the expected cost of operating the system under higher-demand scenarios. Deterministic models that include planning-reserve constraints do not internalize normally the cost of operating the excess capacity that is built to provide the reserves (in the event that these units are needed to serve higher-than-expected demand). As such, the investments that are given by deterministic planning models with planning-reserve constraints tend to be skewed toward technologies that are overly costly to operate. Demand-growth uncertainty can also depend on future technology adoption and electrification rates (*e.g.*, the adoption of electric vehicles).[6] As such, we conduct a sensitivity analysis in Section 5.6 in which the 5% demand increase in the high-demand scenario is increased to up to 50%.

The online supplementary material includes tables that detail further our case-study data, which are excluded here for sake of brevity. All of the cases are programmed using version 21.1.2 of the GAMS mathematical programming language. They are solved using the hybrid branch-and-bound and cutting-plane algorithm in version 12.5.1.0 of the CPLEX solver on a system with Windows 10, a 2.6-GHz processor, and 8 GB of RAM.

## 4. Base-Case Results

Figure 2 summarizes the mix of generation and energy-storage units that are built under a variety of cases with different carbon-emissions limits imposed on the system. The first case that is shown in the figure is a 'business-as-usual' (BAU) case, in which Constraint (12) is relaxed and there is no carbon-emissions limit. The remaining cases impose Constraint (12), with progressively more aggressive carbon-emissions limits that are defined as reductions relative to the BAU case. The final bar in Figure 2 is labeled '100% Reduction'. With our case-study data and the technologies that we consider, complete decarbonization of the power system is very costly. As such, we allow minuscule carbon emissions in the base case and in all of the sensitivity cases that are considered in Section 5. In all of the cases, carbon emissions are reduced by at least 99.7% relative to the BAU case. Nevertheless, we refer to these cases as having 100% carbon reductions. We do not impose a carbon tax in any of these cases, because we assume that explicit carbon-emissions limits are used as the policy mechanism to achieve decarbonization.

[6] https://www.utilitydive.com/news/evs-could-drive-38-rise-in-us-electricity-demand-doe-lab-finds/527358/

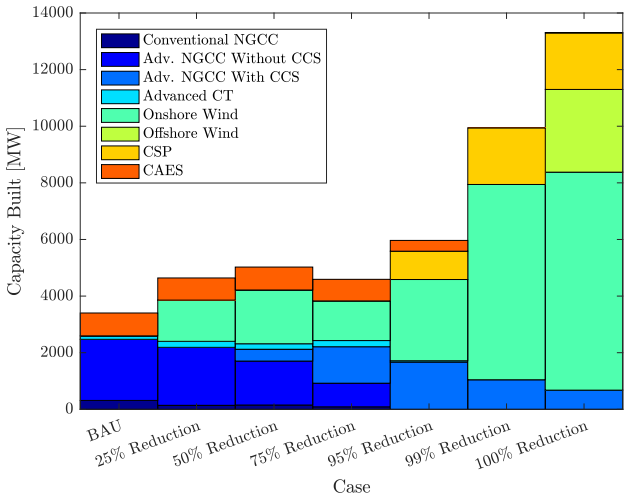


Figure 2: Capacity Built In Business-As-Usual Case and with Different Carbon-Emissions Reductions Relative to Business-As-Usual Case

The BAU case yields investments solely in thermal and energy-storage units. This shows that absent any policy mechanism that internalizes the social cost of carbon, thermal generation is the lowest-cost source of energy. Among the thermal-generation technologies that are available, natural gas-fired units are favored over other generating fuels. Most of the generating capacity in the BAU case is baseload NGCC, with some CAES and advanced CT capacity being built to serve on-peak loads.

As the carbon-emissions limit is enforced and made more stringent, the investment mix changes in a number of ways. 25% carbon-emissions reductions are achieved through greater investments in onshore wind. 50% and 75% carbon-emissions reductions are achieved using onshore wind and by shifting the thermal generation mix toward having CCS. As the thermal-generation mix shifts toward using CCS, there is still a preference for natural gas over coal as a generation fuel. These results show that onshore wind is initially the lowest-cost source of carbon abatement. CCS is only employed with more stringent carbon-reduction goals, once the prime onshore-wind resources are exploited.

The amount of capacity that is built to achieve 75% carbon-emissions reductions is lower than the amount that is built to achieve 25% reductions, which is, in turn, less than the amount that is built to achieve 50% reductions. This result is driven by the trade-off between onshore-wind units and NGCC plants with CCS. With 75% carbon-emissions reductions, the $CO_2$ limit is not so stringent as to make NGCC plants without CCS unviable. As such, NGCC plants without CCS are built in this case (although less capacity is installed compared to the cases with 25% and 50% reductions). Contemporaneously, investments in NGCC plants with CCS increase significantly with 75% carbon-emissions reductions compared to the cases with 25% and 50% reductions. This NGCC with CCS capacity that is added to achieve 75% reductions displaces some onshore-wind units. NGCC plants with CCS are expensive relative to onshore wind. However, NGCC plants provide dispatchable output. Thus, it is economically preferable to use NGCC plants with CCS in place of additional wind capacity to achieve the added emissions reductions beyond the 50% level. Greater carbon-emissions reductions beyond 75% require the use of CSP and offshore wind. This shows that the higher cost of these units, along with the cost of the HVDC connectors that are required to deliver their generation to load, makes these technologies quite expensive. As such, these units are only used with very aggressive carbon-reduction targets. The fact that offshore wind and CSP are built only to achieve carbon-emissions reductions beyond 75% implies also that HVDC lines are built only with these aggressive carbon-reduction goals.

Interestingly, we find that the role of CAES in providing system flexibility diminishes as the carbon-reduction target gets more aggressive. This is because of the carbon emissions that are associated with discharging CAES. As the carbon-emissions limit gets tighter, CAES is replaced with CSP (which has TES

incorporated in it) as the primary source of supply-side flexibility. This diminishing use of CAES as the carbon-emissions limit becomes more stringent results in increasing wind-curtailment rates. Unlike onshore wind and CSP, offshore wind is used only in the most extreme case in which carbon emissions must be eliminated fully. The 'low priority' for building offshore wind stems from its relatively high cost, inflexibility (as TES cannot be incorporated in wind units), and it having little to no advantage over onshore wind in terms of real-time availability. Indeed, the only major benefit to offshore is that its availability is more stable. The distribution of hourly capacity factors of onshore wind has more extremes compared to that of offshore wind.

Figure 2 shows also that as the carbon-emissions limit gets more stringent, the total installed capacity increases considerably (*e.g.*, from 3.4 GW in the BAU case to 13 GW to achieve 100% carbon-emissions reductions). This is because of the lower capacity factor of wind and solar resources compared to dispatchable thermal generation. The 100%-carbon-reduction case results in a very small amount of NGCC with CCS being built. These units have lower emissions rates than CAES and operate only in a small handful of hours when CSP and wind plants are not able to serve fully the load. These small number of hours in which the NGCC units operate give the minuscule carbon emissions in the 100%-carbon-reduction case.

Although nuclear generation has no direct carbon emissions, nuclear capacity is not built in any of the carbon-reduction cases that we examine. This shows that nuclear is an uneconomic generation source in our case study, despite having no carbon footprint. One may attribute the lack of nuclear capacity to its extremely inflexible ramping capability that we assume. However, if it is sufficiently inexpensive, nuclear could be built to serve off-peak loads only, even without the capability to ramp. Doing so would result in the plant having a 100% capacity factor, as it would operate constantly. Moreover, the availability of low-cost CAES could allow even more nuclear capacity to be built to serve on-peak loads. Sioshansi et al. (2012) note that this use of energy storage (*i.e.*, to store nuclear generation overnight to serve on-peak loads) was the major rationale for developing PHS in the United States in the 1970s. The fact that nuclear is not built in any of the cases that we model, even for these limited uses, show that there are substantively lower-cost energy sources, even when seeking carbon-free electricity.

Figure 3 summarizes annual expected operating and investment costs of the system with the different carbon-reduction targets. As expected, enforcing and tightening Constraint (12) increases overall costs. Although the BAU case is the least costly, it is interesting to note that the system can achieve non-trivial carbon-emissions reductions with relatively small overall cost increases relative to BAU. For instance, 25% carbon-emissions reductions can be achieved with only an 8% increase in total expected system costs. On the other hand, complete decarbonization of the electricity sector can be much more costly. 99% emissions reductions increase total expected system costs by 126% (relative to BAU) while complete decarbonization increases costs by 216%.

A question that these cost results raise is the optimal level of decarbonization, taking into account its costs and benefits. The United States Environmental Protection Agency (EPA) produced estimates of the social cost in 2050 of carbon, under different discount rates and carbon-impact scenarios.[7] We can assess the socially optimal level of carbon reduction by relaxing Constraint (12) and setting $\chi$ (*i.e.*, the carbon-emissions price) equal to a given social-cost-of-carbon estimate in (1). Doing so drives the investment model to trade-off the estimated social cost of carbon against the direct cost of achieving carbon reductions. The EPA estimates a social cost of carbon that ranges between \$69/t and \$212/t. These estimates correspond to socially optimal carbon-reduction levels that range between 25% and 85% (relative to the BAU case). Table 2 confirms these findings by reporting the value of the dual variable that is associated with Constraint (12) with different carbon-reduction targets (the results that are reported in the table assume $\chi = 0$). The dual variable that is associated with Constraint (12) gives the marginal cost of carbon-emissions reductions. As expected, the social-cost-of-carbon estimates imply that carbon reductions of up to 85% relative to BAU can be justified economically. Moreover, the table shows that carbon reductions beyond the 85% level result in cost escalations, reaching over \$50000/t for complete decarbonization.

[7] These estimates, which were produced by the EPA under the administration of President Barack Obama, are archived and publicly available at https://19january2017snapshot.epa.gov/climatechange/social-cost-carbon_.html.

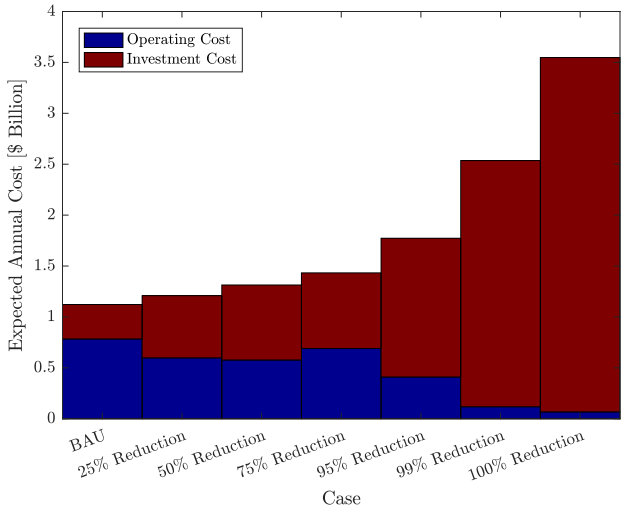


Figure 3: Expected Annual Operating and Investment Costs In Business-As-Usual Case and With Different Carbon-Emissions Reductions Relative to Business-As-Usual Case

Table 2: Marginal Cost of Carbon-Emissions Reductions With Different Carbon-Emissions Reductions Relative to Business-As-Usual Case

| Carbon-Emissions Reduction [% of Emissions in BAU Case] | Marginal Cost of Carbon-Emissions Reductions [$/t] |
|---|---|
| 75 | 94 |
| 85 | 212 |
| 95 | 1063 |
| 99 | 13167 |
| 100 | 53440 |

## 5. Sensitivity Analyses

This section presents the results of six sensitivity analyses, in which we examine the impacts of different case-study assumptions on the design, cost, and operation of the power system. The first sensitivity case, in Section 5.1, considers improvements in the generation, energy-storage, and HVDC technologies. Second, we examine in Section 5.2 the impacts of increased transmission congestion. Next, Section 5.3 analyzes the impacts of relaxing land-use restrictions on building CSP plants. Fourth, Section 5.4 examines the use of PV and BES units for decarbonization. The fifth sensitivity analysis in Section 5.5 considers adiabatic CAES as an alternative to diabatic CAES. Finally, Section 5.6 evaluates the impacts of demand growth.

### *5.1. Technology Improvement*

Our first sensitivity case considers three different technology improvements. The first are efficiency and investment-cost improvements in CSP plants. Lilliestam et al. (2017) examine the historical cost-reduction trajectory of CSP. They find that although CSP has not enjoyed, to date, the same cost reductions that PV solar has, it is beginning to achieve greater reductions. Contemporaneously, Neises and Turchi (2014); Turchi et al. (2013) examine the use of supercritical carbon dioxide power cycles in the power blocks of CSP plants. They find that such power cycles can achieve powerblock efficiencies that are greater than 50%, as opposed to efficiencies ranging between 35% and 45% for the subcritical Rankine cycles that are used in CSP plants today. Based on these findings, we consider a sensitivity case in which the investment costs of CSP plants are 25% lower than in the base case and their efficiencies (which are used to convert the thermal energy that is gathered by the solar fields into electricity-out capacity factors) are increased to 55%.

The second technology improvement involves offshore wind. IEA (2016) finds that offshore wind is costly relative to its onshore counterpart, but that there is potential for this cost difference to be closed. Moreover, offshore wind also suffers from the need for radial HVDC lines to connect generating units to load pockets. Thus, we consider a sensitivity case in which the investment costs of offshore-wind plants are reduced 35% (making their costs comparable to onshore wind) and the cost of HVDC lines are reduced an average of 63%, relative to the base case.

The final technology improvement that we consider is a 10% investment-cost reduction for CAES. This reflects the impacts of learning, which can reduce investment costs as CAES plants are developed around the world in the coming years.

Figure 4 summarizes the capacities of generating and energy-storage units that are built under the technology-improvement sensitivity cases. The bars in the figure are grouped into four sets of three, each of which corresponds to a different technology-improvement case. The first three sets of bars correspond to one of the three technology improvements (*e.g.*, CSP, offshore wind, or CAES) occurring individually. The fourth set of three bars correspond to a case in which all three of the technology improvements occur simultaneously. For each of the four technology-improvement cases, we examine investment decisions under a BAU case and in cases in which carbon emissions are limited to being 50% and 95% less than in the BAU case.[8]

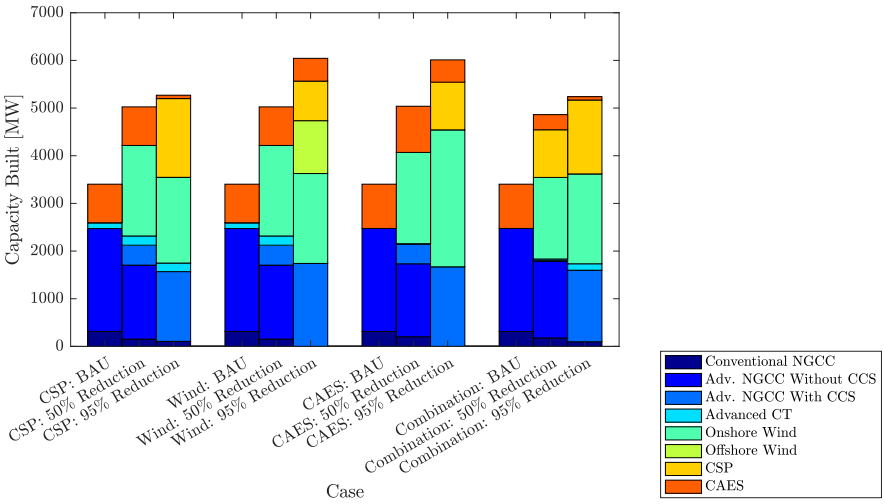


Figure 4: Capacity Built In Business-As-Usual Case and with Different Carbon-Emissions Reductions Relative to Business-As-Usual Case Under Technology-Improvement Sensitivity Analysis

The figure shows that in all of the technology-improvement cases that we examine, none of the renewable technologies are cost-competitive with thermal generation in a BAU case. This indicates that further technology improvements and cost reductions would be needed to make the renewable technologies that we examine cost-competitive with thermal generation in a BAU case. However, if CAES achieves the investment-cost reductions that we examine here, there is a 15% increase in installed CAES capacity in the BAU case. This increased CAES investment comes with the exact same reduction in CT capacity, meaning that CAES is being used to displace this expensive peaking capacity.

The technology-improvement cases that we examine result in some changes in the generation mix as carbon-emissions limits are imposed. Reducing carbon emissions by 50% in any of three individual technology-improvement sensitivity cases gives investment mixes that are similar to that in the base case. In all of these cases, there is investment in onshore wind, which displaces thermal generation, to achieve the

[8]The carbon-emissions limits are defined, in all of the sensitivity cases in this section, relative to the carbon emissions in the corresponding BAU case. Thus, depending upon the technology mix that is built in each BAU case, carbon emissions under each reduction case differ.

requisite carbon reductions. However, the investments are different with 50% carbon-emissions reductions in the 'combined' technology-improvement sensitivity case. The combined case results in less onshore-wind and CAES investments and greater CSP capacity compared to the three sensitivity cases with individual technology improvements. This is due to the combined impact of higher CSP efficiency and lower CSP- and HVDC-investment costs, which make CSP an economic alternative to onshore wind. Moreover, because CSP has integrated TES, the flexibility that this affords reduces the need for CAES. In sum, the CSP displaces close to 200 MW of onshore wind and 500 MW of thermal capacity, relative to the base case.

These trends continue with a 95%-emissions-reduction target. In all of the sensitivity cases, except for the case in which offshore wind *only* achieves technology improvements, CSP has a greater role in decarbonizing the generation mix. Compared to the base case, the combined and CSP-only technology-improvement sensitivity cases result in nearly 1 GW less onshore-wind, 300 MW less CAES, and 600 MW more CSP investments. The fact that 1 GW of wind can be displaced by 600 MW of CSP capacity illustrates further the flexibility benefit that the TES, which is integrated into the CSP plants, provides. When the system relies on wind for decarbonization in the base case, greater capacity must be built to manage the variability in real-time wind availability. The TES systems in the CSP plants reduce the need for such oversizing, as the TES can be used to mitigate the impacts of variable solar availability.

The sensitivity case in which offshore wind *only* has technology improvements results in 1.1 GW of offshore wind being built in place of about 200 MW of CSP (relative to the base case) to achieve 95% emissions reductions. This can be contrasted with the base case, in which offshore wind is built only to achieve complete decarbonization, due to its relatively high cost. Interestingly, no offshore wind is built to achieve 95% emissions reductions in the combined technology-improvement case. This is because, although offshore wind is economically viable in the combined technology-improvement case, so too is CSP, which is less costly and more flexible than offshore wind.

Figure 5 summarizes the annual expected operating and investment costs of the system under the four technology-improvement sensitivity cases. The figure shows that these sensitivity cases yield mixed cost savings. For instance, the combined technology-improvement cases reduces the cost of achieving 50% and 95% emissions reductions by 22% and 33%, respectively, relative to the base case. The case in which CSP *only* has technology improvements reduces the cost of achieving these emissions reductions by 6% and 22%, respectively. This can be contrasted with a case in which offshore wind *only* has technology improvements, which yields only an 8% reduction in the cost of achieving 95% emissions reductions. This follows from the results that are summarized in Figure 4—the combined and CSP-only technology-improvement sensitivity cases yield the most notable differences in the generation mix.

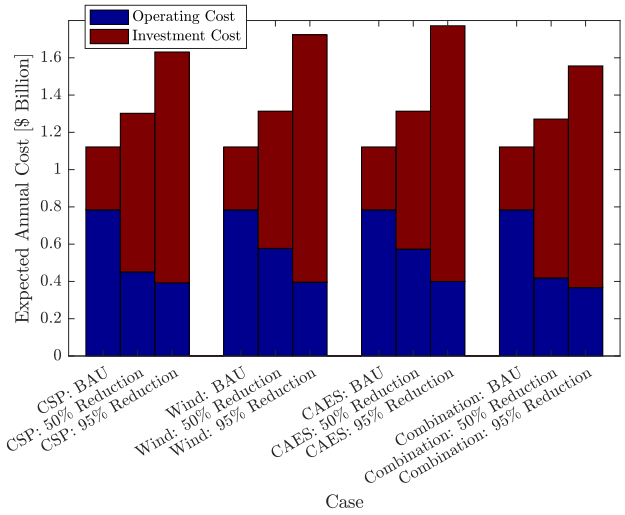


Figure 5: Expected Annual Operating and Investment Costs In Business-As-Usual Case and With Different Carbon-Emissions Reductions Relative to Business-As-Usual Case Under Technology-Improvement Sensitivity Analysis

*5.2. Transmission Congestion*

Our second sensitivity analysis considers the impacts of diminished transmission capacity, which can result from smaller-sized transmission equipment being installed and land-use or other restrictions on building candidate lines. We consider a case in which the transmission capacity of all existing and candidate lines is reduced by 25%. Furthermore, we assume that five of the candidate AC lines, which are close to load pockets in the transmission network, are no longer available to be built.

Figure 6 shows the mix of generation and CAES units that are built in the transmission-congestion sensitivity case with different emissions-reduction targets. Overall, the transmission-congestion sensitivity case results in greater transmission investments and requires more generation and CAES capacity to be built, relative to the base case. The base case does not require new transmission builds until reducing carbon emissions by 95%. Moreover, these transmission builds in the base case are primarily to deliver energy from remote renewable units to loads. Conversely, the transmission-congested sensitivity case requires transmissions builds even in the BAU case. These transmission builds are needed simply to avoid load curtailment. The 99%-carbon-reduction case requires more than double the transmission investment relative to the base case.

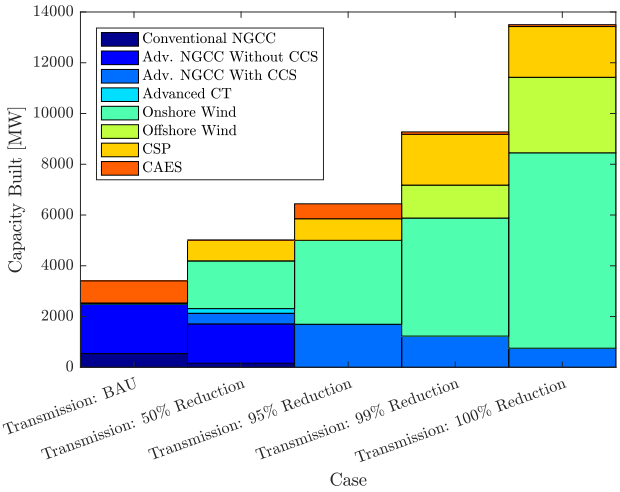


Figure 6: Capacity Built In Business-As-Usual Case and with Different Carbon-Emissions Reductions Relative to Business-As-Usual Case Under Transmission-Congestion Sensitivity Analysis

The generation and CAES units are more dispersed throughout the transmission network than in the base case. Dispersing the energy-production and -storage capacities across the network provides greater flexibility in having energy available in congested load pockets. One benefit of renewable units in this regard is that they are fairly dispersed within the network. As such, renewable and CAES units jointly are able to provide a great deal of congestion relief. One interesting observation regarding the operation of the system in the transmission-constrained case is that energy-storage units at different locations in the network are charged and discharged simultaneously in some hours. This is inefficient, insomuch as energy is lost when it is stored. Simultaneous charging and discharging of energy storage is necessary, nonetheless, because load peaks and troughs occur at different times at different locations. As such, absent transmission capacity, excess energy must be stored at some nodes in the network despite stored energy being discharged to serve load elsewhere in the network.

We analyze the role of the transmission system in abating $CO_2$ emissions by examining a case in which a carbon price of \$100/t is imposed on the system but no explicit carbon constraint is enforced. We find a minuscule 0.22% reduction in carbon emissions and 2.3% higher total costs with the downsized transmission system relative to the base case. These changes are due to the specific network configuration, which disadvantages the use of thermal generation in the transmission-constrained case. Downsizing the transmission system results in some thermal units being offset by 141 MW of additional wind and 110 MW

of additional CAES capacity to handle the added transmission congestion. Because wind and CAES units have lower emissions rates than thermal plants, overall carbon emissions are reduced but costs increase.

### *5.3. Land Use*

The land-use sensitivity case explores further the economic competitiveness of CSP relative to onshore wind. Our base case places CSP at a competitive disadvantage compared to onshore wind, because CSP can only be connected to the network via radial HVDC transmission lines. As such, CSP bears an additional cost compared to onshore wind, which can use existing transmission corridors and can be co-located with load in some cases. The land-use sensitivity case explores the competitiveness of CSP independent of transmission-interconnection costs, by allowing CSP plants to be built at each node where onshore wind can be. These additional candidate CSP plants are assumed to have the same cost and technical characteristics as the CSP units in the base case. We use weather data for 18 additional locations, which correspond to the nodes where onshore wind can be built, to simulate real-time availability of the added candidate CSP plants. We also consider a sensitivity case, which removes the land-use restrictions on building CSP plants and which assumes that CSP achieves the technology improvements that are outlined in Section 5.1.

Figure 7 summarizes the generation and energy-storage capacities that are built with different emissions-reductions targets under the two land-use sensitivity cases. The first set of six bars corresponds to a case in which *only* land-use restrictions on the deployment of CSP are relaxed. The second set of six bars corresponds to a case in which land-use restrictions are relaxed and the CSP-technology improvements that are outlined in Section 5.1 are achieved. The first set of bars shows that even without the cost of interconnecting with the transmission network, CSP is not cost competitive with onshore-wind units. Indeed, the only difference in CSP investments that results from relaxing land-use restrictions is that slightly more capacity is built to achieve 99% emissions reductions. In fact, we find that with land-use restrictions CSP is only built when the capacity to build onshore wind at a particular node is exhausted.

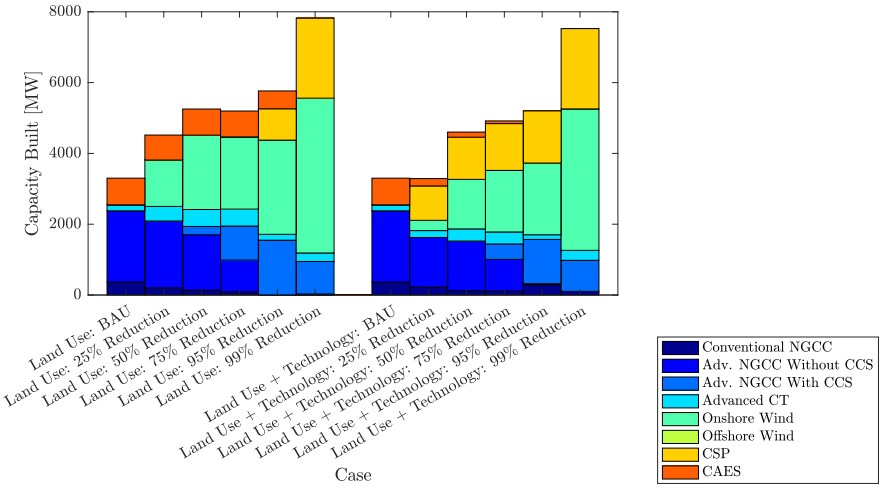


Figure 7: Capacity Built In Business-As-Usual Case and with Different Carbon-Emissions Reductions Relative to Business-As-Usual Case Under Land-Use Sensitivity Analysis

The second set of six bars in Figure 7 shows that this result is reversed if land-use restrictions are relaxed *and* CSP achieves technology improvements. Considerably more CSP capacity is built under these assumptions compared to the base case (and the land-use-*only* sensitivity case) to achieve carbon-emissions reductions between 25% and 95%. Interestingly, the amount of CSP capacity that is built to achieve 99% carbon-emissions reductions is the same with and without the CSP-technology improvements. This suggests that with 99%-carbon-emissions reductions, the CSP that is built is driven primarily by the emissions constraint as opposed to the economics of the technology.

The findings of this sensitivity case are consistent with current experience in the deployment of renewable energy sources. Although CSP has a flexibility benefit relative to wind (and PV solar) that stems from the ability to integrate low-cost TES, CSP has seen little deployment compared to wind. This is largely because CSP is considerably more expensive to build (even when neglecting transmission-interconnection costs). However, our sensitivity cases in which CSP achieves technology improvements (both the case examined here and those in Section 5.1) reveal that CSP has the potential to become competitive with wind.

### *5.4. PV Solar and BES*

This sensitivity analysis examines the benefits of adding PV solar and BES, the characteristics of which are detailed in the online supplementary material, to the set of technologies that are available. Feldman and Margolis (2018) discuss the growth of the global PV market in the past decade and the major cost reductions that the technology has experienced. Moreover, the cost declines of energy-storage technologies are stimulating interest in combining PV with BES units to provide dispatchable energy and reliable capacity. Fu et al. (2018) point to the favorable cost and performance characteristics of the storage medium as a reason for the growing use of lithium-ion batteries in utility-scale PV deployments.

Given this context, this sensitivity case assumes that there are 10 candidate locations between which a total of up to 7 GW of PV can be built. 2.1 GW of this potential capacity is rooftop installations that are co-located with loads and have installation costs ranging between \$1000/kW and \$1012/kW. The remaining 4.9 GW of utility-scale PV has installation costs ranging between \$790/kW and \$801/kW. The PV plants have operating costs that range between \$1.50/MWh and \$1.52/MWh. Solar availability of the PV units is modeled using SAM in the same manner that is outlined in Section 3 for the CSP generators. The PV units are assumed to have DC to AC ratios of 1.2 and 96%-efficient inverters.

Each lithium-ion BES unit, which is co-located with a candidate PV plant, is assumed to have a fixed $\bar{c}_s = 4$ hours of storage capacity. Furthermore, we assume that up to 350 MW of power capacity can be installed in each BES unit. Other characteristics of the BES are taken from the work of Fu et al. (2018). Investment costs range between \$1960/kW and \$2100/kW and are scaled to account for the actual usable SOC range of the battery, which is between 20% and 80% of the nominal battery capacity. Each unit has an operating cost of \$0.50/MWh when charging energy and \$1.00/MWh when discharging. Each BES unit is assumed also to have a 99% roundtrip efficiency and 0.1% hourly self-discharge rate.

Figure 8 summarizes the capacity of generating and energy-storage units that are built when PV solar and BES are added to the set of technologies that can be installed. Interestingly, the figure shows that PV units are cost-competitive with thermal generation in the BAU case. Without any carbon policy in-place in the BAU case, 2.3 GW of PV solar is built to offset 230 MW of thermal capacity and 35 MW of CAES relative to the base case that is discussed in Section 4. This configuration with PV solar is beneficial from environmental and economic perspectives. $CO_2$ emissions and total costs are 25% and 20% lower, respectively, due to PV solar reducing operating costs by 25% with only a 3% increase in investment costs. 770 MW of CAES is still built in the BAU case to serve on-peak demand, because using CAES for peaking purposes is less costly than using BES is.

As the carbon-emissions limit is enforced and tightened, the thermal-generation mix shifts toward the use CCS and PV-solar capacity increases. Carbon-emissions reductions beyond 75% require the use of onshore wind at nodes at which PV cannot be built (or at which all available PV capacity is built). 2.5 GW of onshore wind is built to achieve 95% carbon reductions and 700 MW of BES capacity replaces almost all CAES capacity. Achieving 99% carbon-emissions reductions shows another interesting result: PV-solar and BES capacities both decrease in favor of CSP. Given their relative costs and efficiencies, the TES in CSP provides the preferred source of dispatchability and flexibility to achieve these extreme carbon reductions. This is consistent with the findings of Madaeni et al. (2012). To achieve complete decarbonization, all available CSP capacity is built, more BES capacity is built, and offshore wind enters the generation mix.

### *5.5. Adiabatic CAES*

This sensitivity case considers the use of adiabatic CAES as an alternative to diabatic CAES. Unlike diabatic CAES, adiabatic CAES is a pure energy-storage technology. The primary difference between

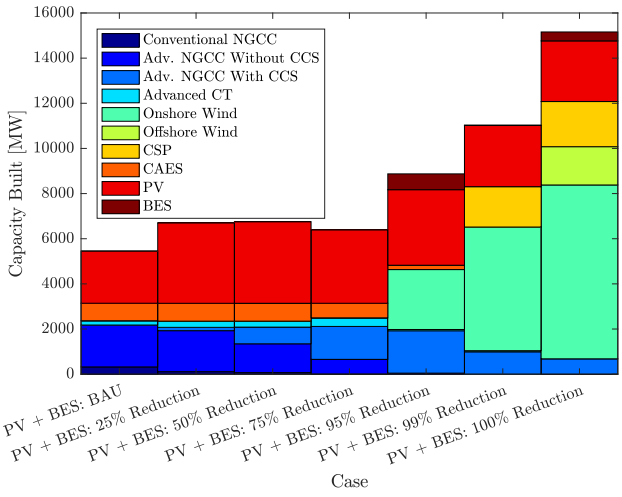


Figure 8: Capacity Built In Business-As-Usual Case and with Different Carbon-Emissions Reductions Relative to Business-As-Usual Case Under PV-Solar-and-BES Sensitivity Analysis

diabatic- and adiabatic-CAES systems is the treatment of the waste heat that is produced when air is compressed in the storage cycle. In a diabatic-CAES system, the waste heat is exhausted to the atmosphere. As such, a diabatic-CAES system must combust natural gas as a heat source when expanding the compressed air in the discharging cycle. An adiabatic-CAES system, conversely, stores the waste heat (often in a dedicated TES system). This stored heat is then combined with the compressed air during the discharging cycle, alleviating the need to use natural gas. This makes adiabatic CAES less costly to operate compared to diabatic CAES. Moreover, adiabatic CAES involves no direct carbon emissions, unlike a diabatic-CAES system, which emits carbon when combusting the natural gas in the discharging cycle. Barbour et al. (2015); Barnes et al. (2015); Hartmann et al. (2012); Liu and Wang (2016); Sciacovelli et al. (2017) provide further details regarding the technical properties and viability of adiabatic CAES.

The adiabatic-CAES sensitivity case assumes that this technology is available in place of diabatic CAES. It is difficult to estimate the technical characteristics of adiabatic CAES, because no commercial-scale systems exist today. Indeed, the DOE Global Energy Storage Database[9] lists the 500 kW Pollegio-Loderio Tunnel Demonstration Plant in Switzerland as the only operational adiabatic CAES plant as of July, 2018. Thus, we rely on current and future estimates of the capabilities of these plants in modeling the adiabatic-CAES sensitivity case.

We assume that the adiabatic-CAES plants have $\bar{c}_s = 10$ hours of storage capacity and that each unit can have up to 350 MW of power capacity built. The adiabatic-CAES units are assumed to have efficiencies of $\eta_s^S = 1.33$, which means that 1.33 MWh of energy must be stored to later discharge 1 MWh of electricity. $\eta_s^S$ being greater than 1 reflects the fact that adiabatic CAES is a pure energy-storage technology, meaning that electricity is lost in the storage cycle. However, the benefit of this energy loss is that the adiabatic-CAES units use no natural gas and have zero carbon emissions.

We consider two sets of investment and operating costs for the adiabatic-CAES plants. The first set, which reflect current cost estimates, assumes investment costs ranging between \$1187/kW and \$1210/kW and charging and discharging costs of \$14/MWh and \$17/MWh, respectively. The second set, which reflect possible future cost reductions, assumes investment costs ranging between \$594/kW and \$605/kW and charging and discharging costs of \$12/MWh and \$13/MWh, respectively.

Figure 9 summarizes the generation and energy-storage capacities that are built in the adiabatic-CAES sensitivity case with different emissions-reduction targets. The first set of bars in the figure corresponds to a case with high investment and operating costs for adiabatic CAES, while the second set corresponds

[9] https://www.energystorageexchange.org/

to lower future cost projections. Interestingly, we find that adiabatic CAES is a less desirable energy-storage technology compared to diabatic CAES. The base case and other sensitivity cases result in some diabatic CAES being built, except with extremely high emissions-reduction targets. This is because once the emissions-reduction target is sufficiently stringent, the carbon emissions that are associated with discharging diabatic CAES makes it use infeasible.

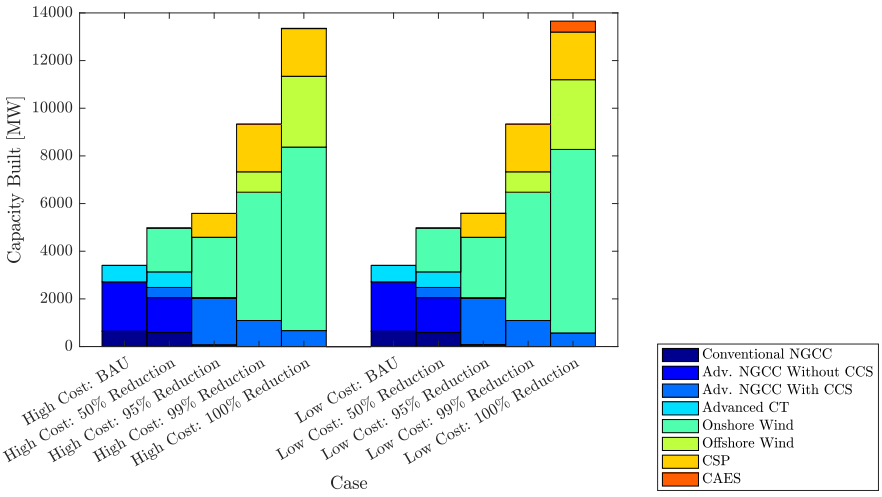


Figure 9: Capacity Built In Business-As-Usual Case and with Different Carbon-Emissions Reductions Relative to Business-As-Usual Case Under Adiabatic-CAES Sensitivity Analysis

Adiabatic CAES relaxes the impact of the emissions-reduction constraint on the use of CAES. However, adiabatic CAES is more costly than diabatic CAES. This cost disadvantage overwhelms the zero-emissions benefit of adiabatic CAES, except in the extreme case of full decarbonization. With full decarbonization, about 10 MW and 500 MW of adiabatic CAES is built with high and low costs, respectively, as opposed to no diabatic CAES in the base case.

### *5.6. Electricity Demand*

According to Mai et al. (2018), electrification and the adoption of electric vehicles may cause electricity demand in the United States to increase over the next three decades. Cooper and Schefter (2017) foresee an additional seven million electric vehicles by 2025 in the United States, compared to the 567000 electric vehicles as of the end of 2016. Rissman (2017) estimates that electric vehicles will compose 60%–75% of total new light-duty vehicle sales in the United States by 2050, at which point they will represent 13%–15% of total national electricity demand.

Given this potential for substantive electricity-demand increases, we conduct a sensitivity analysis on demand growth by modifying the demand levels in the second-stage scenarios. Specifically, we examine three cases in which electricity demands increase by 10%, 30%, and 50% in the high-demand scenario (as opposed to the 5% demand growth that is assumed in the base case that is presented in Sections 3 and 4). The no-demand-growth and low-demand scenarios are not modified in this sensitivity analysis relative to the base case.

Figure 10 shows generation and energy-storage units that are built in the electricity-demand sensitivity case with different emissions-reductions targets. Contrasting this with Figure 2 shows that regardless of the demand-growth level in the high-demand scenario, the technology mix that is built is not altered fundamentally. Instead, the sole substantive impact of demand growth is to 'rescale' the total capacity that is built to serve the possible peak load in the high-demand scenario. This increased capacity translates into higher system costs, which are shown in Figure 11.

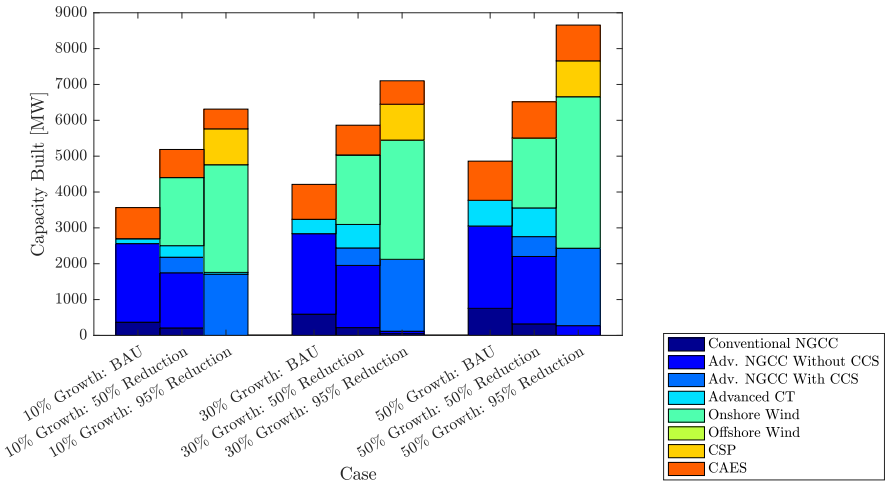


Figure 10: Capacity Built In Business-As-Usual Case and with Different Carbon-Emissions Reductions Relative to Business-As-Usual Case Under Electricity-Demand Sensitivity Analysis

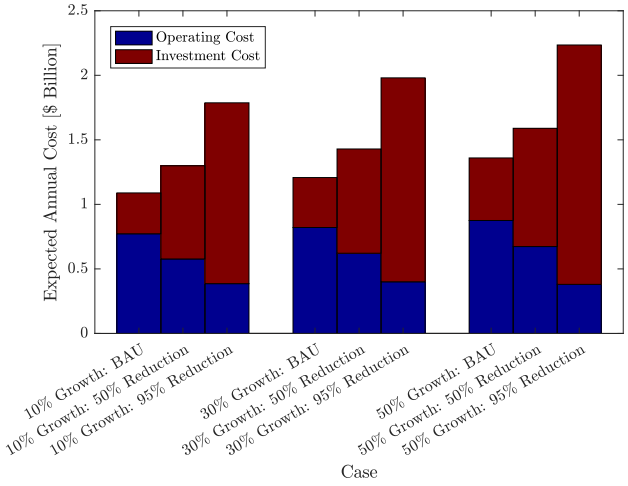


Figure 11: Expected Annual Operating and Investment Costs In Business-As-Usual Case and With Different Carbon-Emissions Reductions Relative to Business-As-Usual Case Under Electricity-Demand Sensitivity Analysis

## 6. Discussion and Conclusions

This paper presents a two-stage stochastic optimization model that can be used for long-term power system-expansion planning. We pay particular attention to modeling carbon-emissions limits and decarbonization of electricity production. This can be achieved in our model using two policy mechanisms: either *via* an explicit carbon-emissions constraint or by pricing carbon (*e.g.*, Pigouvian taxes on emissions). Our model and case study consider three technical options for decarbonization—renewable energy sources, nuclear generators, and fossil-fueled plants with integrated CCS systems.

Weather-dependent renewable generators raise modeling, planning, and operating challenges, because their real-time resource availability is uncertain and variable. As such, we include energy-storage technologies in the model as a flexibility source for mitigating these characteristics of renewables. We focus on two energy-storage technologies—CAES and TES integrated in CSP plants—in our base case, which can be deployed widely in high-renewable-penetration scenarios. The real-time variability of renewable availability is captured in our model using a variety of different operating conditions. These operating conditions capture

the range of weather conditions over the course of a year, which can give different load levels and wind and solar availabilities. Large-scale uncertainties, such as long-term load growth, are captured explicitly through second-stage scenarios in the scenario tree.

We demonstrate our model and analyze decarbonization pathways using a detailed case study that is based on the ERCOT system. We find that absent any policy mechanism that internalizes the societal cost of carbon, the power system still maintains a fossil-fueled generation mix with some CAES to alleviate the need to build peaking generation capacity. Natural gas is preferred to coal as a generation fuel, given its anticipated low cost and the high efficiency of NGCC units. This system design holds regardless of potential future cost reductions in renewable and CAES technologies. However, when investments in PV solar and BES units are allowed, 2.3 GW of PV-solar capacity is installed and displaces 230 MW of thermal and 35 MW of CAES in the BAU case. This provides both economic and environmental benefits and shows that PV solar is indeed cost-competitive with thermal generation absent any carbon policy.

As the social cost of carbon is internalized (we do this in our case study *via* explicit carbon-emissions limits) the system moves away from natural gas-fired generators toward onshore-wind and (when allowed) PV solar capacity. Moreover, portions of the natural gas-fired fleet use CCS for modest carbon-emissions limits. As the carbon-emissions limits become very stringent, fossil-fueled generation essentially is phased out of the system completely. CAES is also phased out, because of the carbon emissions that are associated with the combustion of natural gas in the discharging cycle. The flexibility that CAES affords is instead provided by CSP plants, which have TES incorporated in them. Finally, achieving complete decarbonization of the electric power system calls upon the use of offshore wind, which tends to be more costly than onshore with only marginal relative improvements in its capacity factor. CSP plants are preferred to PV solar and BES to achieve extreme decarbonization. Interestingly, nuclear is not used for decarbonization purposes, given its very high cost.

Achieving modest decarbonization targets yields relatively small expected power system-cost increases. Indeed, we find that for a wide range of social costs of carbon, reducing carbon emissions by between 25% and 85% (relative to a BAU case) is socially optimal. One of the challenges in setting carbon policy is that the social costs of climate change are difficult to estimate *a priori*. Thus, it may prove robust against the potential for catastrophic impacts of climate change to set decarbonization targets that are toward the upper end of this range.

Under current estimates of costs and technical characteristics, onshore wind and solar PV are the most attractive renewable-energy technologies that we consider. We find, however, that if CSP achieves its projected cost reductions and efficiency gains and if transmission-interconnection costs are reduced, CSP can become an extremely competitive alternative to onshore wind. Moreover, the inherent flexibility of CSP alleviates the need to build stand-alone energy-storage capacity. Offshore wind is not competitive with onshore wind and CSP. This is because of its relatively high investment and operating costs and the need to build radial HVDC lines to connect it to load centers. For these reasons, offshore wind is built only if all other renewable-energy sources are exhausted.

Diabatic CAES is an economically feasible alternative to PHS. This is an important finding, because many parts of the world lack either the water or geological formations that are necessary for the deployment of PHS. Conversely, CAES has the potential to be deployed in many renewable-rich regions. The major difficulty that diabatic CAES raises is the emission of carbon that is associated with the discharging cycle. Adiabatic CAES, which is a technology that is currently in the demonstration phase, holds the potential to mitigate the carbon-emissions issue of diabatic CAES. However, our adiabatic-CAES sensitivity case reveals that with current and future projections of technology costs, adiabatic CAES is not an economic source of supply-side flexibility. Our findings suggest that adiabatic CAES requires further development to become a viable alternative to diabatic CAES, except under extreme carbon-reduction targets.

Our analysis focuses on using energy storage as a source of supply-side flexibility to achieve supply/demand balance. One could also consider the use of demand-side flexibility, for instance through demand response, as a means of achieving this balance. The use of demand response is an area of future research that is beyond the scope of our current work. The methodology that Sioshansi (2010) uses to examine the renewable-integration benefits of demand response likely could be adapted within the modeling framework that we develop here.

Our analysis shows that demand growth does not affect the optimal mix of technologies that are built. Rather, demand growth results in scaling up the total capacity that is installed with a commensurate increase in system costs.

## Acknowledgments

We thank the editors and two anonymous reviewers for helpful comments and suggestions that improved the quality of this paper. The third author thanks Armin Sorooshian for the same. The material in this paper is based upon work financially supported by the National Science Foundation through Grant Number 1548015. The opinions that are expressed in this paper are those of the authors. They do not represent necessarily the views or official positions of Engie Italia and do not commit Engie Italia to any course of action in the future.

## References

Barbour, E., Mignard, D., Ding, Y., Li, Y., 1 October 2015. Adiabatic Compressed Air Energy Storage with packed bed thermal energy storage. Applied Energy 155, 804–815.

Baringo, L., Conejo, A. J., January 2013. Correlated wind-power production and electric load scenarios for investment decisions. Applied Energy 101, 475–482.

Barnes, F. S., Budd, D. A., Lim, M., Freeman, E. R., June 2015. Compressed Air Energy Storage (CAES). In: Cabeza, L. F., Sioshansi, R., Yan, J. (Eds.), Handbook of Clean Energy Systems. Vol. 5, Energy Storage. John Wiley & Sons Ltd, West Sussex, United Kingdom, Ch. 19, pp. 2717–2742.

Blair, N., Dobos, A. P., Freeman, J., Neises, T., Wagner, M., Ferguson, T., Gilman, P., Janzou, S., February 2014. System Advisor Model, SAM 2014.1.14: General Description. Tech. Rep. NREL/TP-6A20-61019, National Renewable Energy Laboratory, Golden, CO.

Calderón, S., Alvarez, A. C., Loboguerrero, A. M., Arango, S., Calvin, K., Kober, T., Daenzer, K., Fisher-Vanden, K., May 2016. Achieving $CO_2$ reductions in Colombia: Effects of carbon taxes and abatement targets. Energy Economics 56, 575–586.

Conejo, A. J., Morales, L. B., Kazempour, S. J., Siddiqui, A. S., 2016. Investment in Electricity Generation and Transmission: Decision Making under Uncertainty. Vol. 205. Springer International Publishing, Cham, Switzerland.

Cooper, A., Schefter, K., June 2017. Plug-in Electric Vehicle Sales Forecast Through 2025 and the Charging Infrastructure Required. Tech. rep., The Edison Foundation Institute for Electric Innovation and Edison Electric Institute, Washington, DC.

Das, T., Krishnan, V., Gu, Y., McCalley, J. D., 24-29 July 2011. Compressed Air Energy Storage: State Space Modeling and Performance Analysis. In: 2011 IEEE Power & Energy Society General Meeting. Institute of Electrical and Electronics Engineers, San Diego, CA.

de Maere d'Aertrycke, G., Ehrenmann, A., Smeers, Y., June 2017. Investment with incomplete markets for risk: The need for long-term contracts. Energy Policy 105, 571–583.

Denholm, P., Ela, E., Kirby, B., Milligan, M. R., January 2010. The Role of Energy Storage with Renewable Electricity Generation. Tech. Rep. NREL/TP-6A2-47187, National Renewable Energy Laboratory, Golden, CO.

Di Sbroiavacca, N., Nadal, G., Lallana, F., Falzon, J., Calvin, K., May 2016. Emissions reduction scenarios in the Argentinean Energy Sector. Energy Economics 56, 552–563.

Domínguez, R., Conejo, A. J., Carrión, M., January 2015. Toward Fully Renewable Electric Energy Systems. IEEE Transactions on Power Systems 30, 316–326.

Draxl, C., Clifton, A., Hodge, B.-M., McCaa, J., 1 August 2015a. The Wind Integration National Dataset (WIND) Toolkit. Applied Energy 151, 353–366.

Draxl, C., Hodge, B.-M., Clifton, A., McCaa, J., April 2015b. Overview and Meteorological Validation of the Wind Integration National Dataset Toolkit. Tech. Rep. NREL/TP-5000-61740, National Renewable Energy Laboratory, Golden, CO.

Drury, E., Denholm, P., Sioshansi, R., August 2011. The Value of Compressed Air Energy Storage in Energy and Reserve Markets. Energy 36, 4959–4973.

EIA, 5 January 2017. Annual Energy Outlook 2017. U.S. Energy Information Administration, DOE/EIA-0383 (2017) Edition.

Feldman, D., Margolis, R., August 2018. Q1/Q2 2018 Solar Industry Update. Tech. Rep. NREL/PR-6A20-72036, National Renewable Energy Laboratory, Golden, CO.

Fu, R., Remo, T., Margolis, R., November 2018. 2018 U.S. Utility-Scale Photovoltaics-Plus-Energy Storage System Costs Benchmark. Tech. Rep. NREL/TP-6A20-71714, National Renewable Energy Laboratory, Golden, CO.

Graf, C., Marcantonini, C., August 2017. Renewable energy and its impact on thermal generation. Energy Economics 66, 421–430.

Graves, F., Jenkin, T., Murphy, D., October 1999. Opportunities for Electricity Storage in Deregulating Markets. The Electricity Journal 12, 46–56.

Greenblatt, J. B., Succar, S., Denkenberger, D. C., Williams, R. H., Socolow, R. H., March 2007. Baseload wind energy: modeling the competition between gas turbines and compressed air energy storage for supplemental generation. Energy Policy 35, 1474–1492.

Hartmann, N., Vöhringer, O., Kruck, C., Eltrop, L., May 2012. Simulation and analysis of different adiabatic Compressed Air Energy Storage plant configurations. Applied Energy 93, 541–548.
IEA, 25 October 2016. Medium-Term Renewable Energy Market Report 2016. International Energy Agency, 9 rue de la Fédération, 75739 Paris Cedex 15, France.
King, J., Clifton, A., Hodge, B.-M., September 2014. Validation of Power Output for the WIND Toolkit. Tech. Rep. NREL/TP-5D00-61714, National Renewable Energy Laboratory, Golden, CO.
Krohn, S., Morthorst, P.-E., Awerbuch, S., March 2009. The Economics of Wind Energy. Tech. rep., European Wind Energy Association.
Lilliestam, J., Labordena, M., Patt, A., Pfenninger, S., July 2017. Empirically observed learning rates for concentrating solar power and their responses to regime change. Nature Energy 2, 1–6.
Liu, J.-L., Wang, J.-H., 15 January 2016. A comparative research of two adiabatic compressed air energy storage systems. Energy Conversion and Management 108, 566–578.
Liu, Y., Sioshansi, R., Conejo, A. J., May 2018a. Hierarchical Clustering to Find Representative Operating Periods for Capacity-Expansion Modeling. IEEE Transactions on Power Systems 33, 3029–3039.
Liu, Y., Sioshansi, R., Conejo, A. J., January 2018b. Multistage Stochastic Investment Planning with Multiscale Representation of Uncertainties and Decisions. IEEE Transactions on Power Systems 33, 781–791.
MacQueen, J., 1967. Some methods for classification and analysis of multivariate observations. In: Proceedings of the Fifth Berkeley Symposium on Mathematical Statistics and Probability. Vol. 1. pp. 281–297.
Madaeni, S. H., Sioshansi, R., Denholm, P., February 2012. How Thermal Energy Storage Enhances the Economic Viability of Concentrating Solar Power. Proceedings of the IEEE 100, 335–347.
Mai, T., Jadun, P., Logan, J., McMillan, C., Muratori, M., Steinberg, D., Vimmerstedt, L., Jones, R., Haley, B., Nelson, B., June 2018. Electrification Futures Study: Scenarios of Electric Technology Adoption and Power Consumption for the United States. Tech. Rep. NREL/TP-6A20-71500, National Renewable Energy Laboratory, Golden, CO.
Neises, T. W., Turchi, C. S., 2014. A Comparison of Supercritical Carbon Dioxide Power Cycle Configurations with an Emphasis on CSP Applications. Energy Procedia 49, 1187–1196.
Qi, T., Weng, Y., Zhang, X., He, J., November 2016. An analysis of the driving factors of energy-related $CO_2$ emission reduction in China from 2005 to 2013. Energy Economics 60, 15–22.
Rissman, J., September 2017. The Future of Electric Vehicles in the U.S. Tech. rep., Energy Innovation: Policy and Technology LLC, San Francisco, CA.
Sciacovelli, A., Li, Y., Chen, H., Wu, Y., Wang, J., Garvey, S., Ding, Y., 1 January 2017. Dynamic simulation of Adiabatic Compressed Air Energy Storage (A-CAES) plant with integrated thermal storage  Link between components performance and plant performance. Applied Energy 185 Part 1, 16–28.
Sengupta, M., Habte, A., Gotseff, P., Weekley, A., Lopez, A., Anderberg, M., Molling, C., Heidinger, A., September 2014a. A Physics-Based GOES Product for Use in NREL's National Solar Radiation Database. Tech. Rep. NREL/CP-5D00-62776, National Renewable Energy Laboratory, Golden, CO.
Sengupta, M., Habte, A., Gotseff, P., Weekley, A., Lopez, A., Molling, C., Heidinger, A., July 2014b. A Physics-Based GOES Satellite Product for Use in NREL's National Solar Radiation Database. Tech. Rep. NREL/CP-5D00-62237, National Renewable Energy Laboratory, Golden, CO.
Sioshansi, R., April 2010. Evaluating the Impacts of Real-Time Pricing on the Cost and Value of Wind Generation. IEEE Transactions on Power Systems 25, 741–748.
Sioshansi, R., Denholm, P., February 2010a. The Value of Concentrating Solar Power and Thermal Energy Storage. Tech. Rep. NREL/TP-6A2-45833, National Renewable Energy Laboratory, Golden, CO.
Sioshansi, R., Denholm, P., October 2010b. The Value of Concentrating Solar Power and Thermal Energy Storage. IEEE Transactions on Sustainable Energy 1, 173–183.
Sioshansi, R., Denholm, P., Jenkin, T., January 2011. A Comparative Analysis of the Value of Pure and Hybrid Electricity Storage. Energy Economics 33, 56–66.
Sioshansi, R., Denholm, P., Jenkin, T., March 2012. Market and Policy Barriers to Deployment of Energy Storage. Economics of Energy & Environmental Policy 1, 47–63.
Sioshansi, R., Denholm, P., Jenkin, T., Weiss, J., March 2009. Estimating the Value of Electricity Storage in PJM: Arbitrage and Some Welfare Effects. Energy Economics 31, 269–277.
Succar, S., Greenblatt, J. B., Denkenberger, D. C., Williams, R. H., June 4-7 2006. An Integrated Optimization Of Large-Scale Wind With Variable Rating Coupled To Compressed Air Energy Storage. In: Windpower 2006. American Wind Energy Association, Pittsburgh, Pennsylvania.
Succar, S., Williams, R. H., April 2008. Compressed Air Energy Storage Theory, Resources, And Applications For Wind Power. Tech. rep., Princeton Environmental Institute.
Turchi, C. S., Ma, Z., Neises, T. W., Wagner, M. J., 1 November 2013. Thermodynamic Study of Advanced Supercritical Carbon Dioxide Power Cycles for Concentrating Solar Power Systems. Journal of Solar Energy Engineering 135, 041007.
Vaillancourt, K., April 2014. Electricity Transmission and Distribution. Energy Technology Systems Analysis Program E12, International Energy Agency.

# Supplementary Material: A Two-Stage Stochastic Optimization Planning Framework to Decarbonize Deeply Electric Power Systems

Luigi Boffino Antonio J. Conejo Ramteen Sioshansi Giorgia Oggioni

## 1 Introduction

This document provides all of the detailed input data that are used in the base-case and sensitivity analyses in the paper "A Two-Stage Stochastic Optimization Planning Framework to Decarbonize Deeply Electric Power Systems." All of the investment costs are overnight costs, which must be annualized (we use an 11% annualization rate in our analysis).

## 2 Data For Base Case

Table 1: Technical Characteristics of Onshore-Wind Units

| Node | Maximum Capacity [MW] | Operating Cost [$/MWh] | Investment Cost [$/kW] |
|---|---|---|---|
| 1 | 700 | 2.71 | 2005 |
| 7 | 700 | 2.15 | 2022 |
| 13 | 700 | 2.06 | 1980 |
| 13 | 700 | 2.05 | 2010 |
| 14 | 700 | 2.10 | 1990 |
| 14 | 700 | 2.21 | 2020 |
| 16 | 700 | 2.04 | 2040 |
| 18 | 700 | 2.00 | 2100 |
| 21 | 700 | 2.04 | 2000 |
| 22 | 700 | 2.55 | 1970 |
| 23 | 700 | 2.02 | 1980 |

Table 2: Technical Characteristics of Offshore-Wind Units

| Node | Maximum Capacity [MW] | Operating Cost [$/MWh] | Investment Cost [$/kW] |
|---|---|---|---|
| 25 | 2000 | 4.85 | 3190 |
| 27 | 2000 | 5.35 | 2900 |

Table 3: Technical Characteristics of CSP Units

| Node | Maximum Capacity [MW] | Generation Cost [$/MWh] | TES-Discharging Cost [$/MWh] | TES-Charging Cost [$/MWh] | Investment Cost [$/kW] |
|---|---|---|---|---|---|
| 26 | 1000 | 4.00 | 0.1400 | 0.1549 | 3272 |
| 28 | 1000 | 3.80 | 0.1400 | 0.1549 | 3599 |

Table 4: Technical Characteristics of Diabatic-CAES Units

| Node | Maximum Capacity [MW] | Discharging Cost [$/MWh] | Charging Cost [$/MWh] | Investment Cost [$/kW] | Carbon-Emissions Rate of Discharging [t/MWh] |
|---|---|---|---|---|---|
| 1 | 350 | 28.79 | 0.5 | 571 | 0.259 |
| 7 | 350 | 28.71 | 0.5 | 560 | 0.259 |
| 13 | 350 | 28.33 | 0.5 | 599 | 0.259 |
| 14 | 350 | 28.47 | 0.5 | 550 | 0.259 |
| 16 | 350 | 28.55 | 0.5 | 605 | 0.259 |
| 21 | 350 | 28.66 | 0.5 | 610 | 0.259 |
| 22 | 350 | 28.75 | 0.5 | 589 | 0.259 |
| 23 | 350 | 28.41 | 0.5 | 600 | 0.259 |

Table 5: Technical Characteristics of Existing Transmission Lines

| From Node | To Node | Reactance [p.u.] | Flow Limit [MW] |
|---|---|---|---|
| 1 | 2 | 0.014 | 450 |
| 1 | 3 | 0.211 | 220 |
| 1 | 5 | 0.085 | 510 |
| 1 | 23 | 0.087 | 600 |
| 2 | 4 | 0.127 | 220 |
| 2 | 6 | 0.192 | 220 |
| 3 | 9 | 0.119 | 400 |
| 3 | 24 | 0.084 | 400 |
| 4 | 9 | 0.104 | 220 |
| 5 | 10 | 0.088 | 220 |
| 6 | 10 | 0.061 | 200 |
| 7 | 8 | 0.061 | 320 |
| 8 | 9 | 0.165 | 220 |
| 8 | 10 | 0.165 | 220 |
| 9 | 11 | 0.084 | 320 |
| 9 | 12 | 0.084 | 250 |
| 10 | 11 | 0.084 | 230 |
| 10 | 12 | 0.084 | 200 |
| 11 | 13 | 0.048 | 400 |
| 11 | 14 | 0.042 | 320 |
| 12 | 13 | 0.048 | 400 |
| 12 | 23 | 0.097 | 600 |
| 14 | 16 | 0.059 | 600 |
| 15 | 16 | 0.071 | 600 |
| 15 | 21 | 0.049 | 600 |
| 15 | 21 | 0.049 | 600 |
| 15 | 24 | 0.052 | 310 |
| 16 | 17 | 0.026 | 800 |
| 16 | 19 | 0.023 | 600 |
| 17 | 18 | 0.014 | 600 |
| 17 | 22 | 0.105 | 600 |
| 18 | 21 | 0.026 | 600 |
| 18 | 21 | 0.026 | 600 |
| 19 | 20 | 0.040 | 600 |
| 19 | 20 | 0.040 | 600 |
| 20 | 23 | 0.022 | 600 |
| 20 | 23 | 0.022 | 600 |
| 21 | 22 | 0.068 | 600 |

Table 6: Technical Characteristics of Candidate AC Transmission Lines

| From Node | To Node | Reactance [p.u.] | Flow Limit [MW] | Investment Cost [$ million] |
|---|---|---|---|---|
| 1 | 9 | 0.026 | 600 | 210 |
| 3 | 15 | 0.026 | 600 | 200 |
| 3 | 18 | 0.049 | 400 | 312 |
| 7 | 10 | 0.026 | 600 | 201 |
| 9 | 14 | 0.026 | 600 | 190 |
| 9 | 21 | 0.049 | 400 | 315 |
| 10 | 11 | 0.026 | 600 | 180 |
| 10 | 13 | 0.026 | 600 | 195 |
| 12 | 22 | 0.049 | 400 | 290 |
| 16 | 17 | 0.026 | 800 | 190 |

Table 7: Technical Characteristics of Candidate HVDC Transmission Lines

| From Node | To Node | Flow Limit [MW] | Investment Cost [$ million] |
|---|---|---|---|
| 25 | 6 | 2000 | 684.0 |
| 25 | 8 | 2000 | 817.5 |
| 25 | 13 | 2000 | 589.5 |
| 25 | 22 | 2000 | 503.5 |
| 26 | 3 | 1000 | 503.5 |
| 26 | 15 | 1000 | 551.0 |
| 26 | 16 | 1000 | 589.0 |
| 26 | 17 | 1000 | 617.5 |
| 27 | 6 | 2000 | 532.0 |
| 27 | 8 | 2000 | 551.0 |
| 27 | 13 | 2000 | 503.5 |
| 28 | 1 | 1000 | 817.5 |
| 28 | 3 | 1000 | 684.0 |
| 28 | 15 | 1000 | 589.5 |
| 28 | 18 | 2000 | 503.5 |

# 3 Data For Sensitivity Cases

## 3.1 Data For Technology-Improvement Sensitivity Case

Table 8: Investment Costs of Candidate HVDC Transmission Lines

| From Node | To Node | Investment Cost [$ million] |
|---|---|---|
| 25 | 6 | 304.0 |
| 25 | 8 | 437.0 |
| 25 | 13 | 209.0 |
| 25 | 22 | 123.5 |
| 26 | 3 | 123.5 |
| 26 | 15 | 171.0 |
| 26 | 16 | 209.0 |
| 26 | 17 | 237.5 |
| 27 | 6 | 152.0 |
| 27 | 8 | 171.0 |
| 27 | 13 | 123.5 |
| 28 | 1 | 437.5 |
| 28 | 3 | 304.5 |
| 28 | 15 | 209.0 |
| 28 | 18 | 123.5 |

## 3.2 Data For Land-Use Sensitivity Case

Table 9: Technical Characteristics of Additional CSP Units in Land-Use Sensitivity Case

| Node | Maximum Capacity [MW] | Generation Cost [$/MWh] | TES-Discharging Cost [$/MWh] | TES-Charging Cost [$/MWh] | Investment Cost [$/kW] |
|---|---|---|---|---|---|
| 1 | 350 | 3.86 | 0.14 | 0.1549 | 3507 |
| 7 | 350 | 3.87 | 0.14 | 0.1549 | 3442 |
| 13 | 350 | 3.86 | 0.14 | 0.1549 | 3336 |
| 13 | 350 | 3.81 | 0.14 | 0.1549 | 3471 |
| 14 | 350 | 3.88 | 0.14 | 0.1549 | 3513 |
| 14 | 350 | 3.85 | 0.14 | 0.1549 | 3350 |
| 16 | 350 | 3.87 | 0.14 | 0.1549 | 3239 |
| 18 | 350 | 3.85 | 0.14 | 0.1549 | 3345 |
| 21 | 350 | 3.82 | 0.14 | 0.1549 | 3432 |
| 22 | 350 | 3.83 | 0.14 | 0.1549 | 3222 |
| 23 | 350 | 3.89 | 0.14 | 0.1549 | 3417 |
| 26 | 1000 | 4.00 | 0.14 | 0.1549 | 3599 |
| 28 | 1000 | 3.80 | 0.14 | 0.1549 | 3272 |

Table 10: Technical Characteristics of Additional CSP Units in Land-Use Sensitivity Case With Technology Improvements

| Node | Maximum Capacity [MW] | Generation Cost [$/MWh] | TES-Discharging Cost [$/MWh] | TES-Charging Cost [$/MWh] | Investment Cost [$/kW] |
|---|---|---|---|---|---|
| 1 | 350 | 3.86 | 0.14 | 0.1549 | 2630 |
| 7 | 350 | 3.87 | 0.14 | 0.1549 | 2581 |
| 13 | 350 | 3.86 | 0.14 | 0.1549 | 2502 |
| 13 | 350 | 3.81 | 0.14 | 0.1549 | 2603 |
| 14 | 350 | 3.88 | 0.14 | 0.1549 | 2634 |
| 14 | 350 | 3.85 | 0.14 | 0.1549 | 2512 |
| 16 | 350 | 3.87 | 0.14 | 0.1549 | 2429 |
| 18 | 350 | 3.85 | 0.14 | 0.1549 | 2508 |
| 21 | 350 | 3.82 | 0.14 | 0.1549 | 2574 |
| 22 | 350 | 3.83 | 0.14 | 0.1549 | 2416 |
| 23 | 350 | 3.89 | 0.14 | 0.1549 | 2562 |
| 26 | 1000 | 4.00 | 0.14 | 0.1549 | 2699 |
| 28 | 1000 | 3.8 | 0.14 | 0.1549 | 2454 |

## 3.3 Data For Adiabatic-CAES Sensitivity Case

Table 11: Technical Characteristics of Adiabatic-CAES Units With High Costs

| Node | Maximum Capacity [MW] | Discharging Cost [$/MWh] | Charging Cost [$/MWh] | Investment Cost [$/kW] |
|---|---|---|---|---|
| 1 | 350 | 14 | 17 | 1198 |
| 7 | 350 | 14 | 17 | 1187 |
| 13 | 350 | 14 | 17 | 1199 |
| 14 | 350 | 14 | 17 | 1210 |
| 16 | 350 | 14 | 17 | 1195 |
| 21 | 350 | 14 | 17 | 1205 |
| 22 | 350 | 14 | 17 | 1189 |
| 23 | 350 | 14 | 17 | 1200 |

Table 12: Technical Characteristics of Adiabatic-CAES Units With Low Costs

| Node | Maximum Capacity [MW] | Discharging Cost [$/MWh] | Charging Cost [$/MWh] | Investment Cost [$/kW] |
|---|---|---|---|---|
| 1 | 350 | 11.5 | 12.5 | 599 |
| 7 | 350 | 11.5 | 12.5 | 593 |
| 13 | 350 | 11.5 | 12.5 | 599 |
| 14 | 350 | 11.5 | 12.5 | 605 |
| 16 | 350 | 11.5 | 12.5 | 597 |
| 21 | 350 | 11.5 | 12.5 | 602 |
| 22 | 350 | 11.5 | 12.5 | 504 |
| 23 | 350 | 11.5 | 12.5 | 600 |

## 3.4 Data For PV and BES Sensitivity Case

Table 13: Technical Characteristics of BES Units

| Node | Maximum Capacity [MW] | Discharging Cost [$/MWh] | Charging Cost [$/MWh] | Investment Cost [$/kW] |
|---|---|---|---|---|
| 1 | 350 | 1 | 0.5 | 1990 |
| 3 | 350 | 1 | 0.5 | 1960 |
| 5 | 350 | 1 | 0.5 | 1971 |
| 7 | 350 | 1 | 0.5 | 1989 |
| 10 | 350 | 1 | 0.5 | 2012 |
| 14 | 350 | 1 | 0.5 | 2100 |
| 16 | 350 | 1 | 0.5 | 2090 |
| 18 | 350 | 1 | 0.5 | 2000 |
| 22 | 350 | 1 | 0.5 | 1955 |
| 23 | 350 | 1 | 0.5 | 2010 |

Table 14: Technical Characteristics of PV-Solar Units

| Node | Maximum Capacity [MW] | Operating Cost [$/MWh] | Investment Cost [$/kW] |
|---|---|---|---|
| 1 | 700 | 1.530 | 799 |
| 3 | 700 | 1.520 | 1000 |
| 5 | 700 | 1.521 | 1010 |
| 7 | 700 | 1.521 | 795 |
| 10 | 700 | 1.520 | 1012 |
| 14 | 700 | 1.511 | 798 |
| 16 | 700 | 1.510 | 801 |
| 18 | 700 | 1.500 | 790 |
| 22 | 700 | 1.531 | 800 |
| 23 | 700 | 1.540 | 792 |